Neuronal Excitability

Abnormal UP/DOWN Membrane Potential Dynamics Coupled with the Neocortical Slow Oscillation in Dentate Granule Cells during the Latent Phase of Temporal Lobe Epilepsy[1,2,3]

David W. Ouedraogo,[1,2,3] Pierre-Pascal Lenck-Santini[1,2,3,4], Geoffrey Marti[1,2,3,5], David Robbe,[1,2,3] Valérie Crépel,[1,2,3] and Jérôme Epsztein[1,2,3]

[1]Institut National de la Santé et de la Recherche Médicale U901, 13273 Marseille, France, [2]Unité Mixte de Recherche 901, Aix-Marseille University, 13273 Marseille, France, [3]Institut de neurobiologie de la méditerranée, 13273 Marseille, France, [4]Department of Neurological Sciences, University of Vermont, Burlington, Vermont 05405, [5]Centre National de la Recherche Scientifique, Institut des Sciences du Mouvement, Unité Mixte de Recherche 7287, Aix-Marseille University, 13288 Marseille, France

Visual Abstract
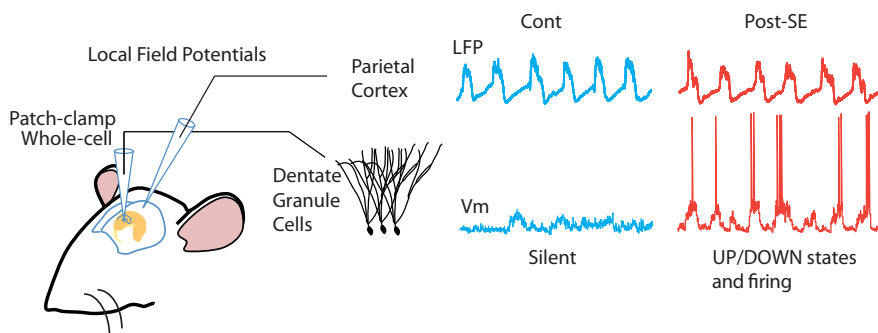
The dentate gyrus, a major entry point to the hippocampus, gates (or filters) incoming information from the cortex. During sleep or anesthesia, the slow-wave oscillation (SWO) orchestrates hippocampus–neocortex communication, which is important for memory formation. The dentate gate is altered in temporal lobe epilepsy (TLE) early during epileptogenesis, which favors the propagation of pathological activities. Yet, whether the gating of physiological SWO by dentate granule cells (DGCs) is altered in TLE has remained unexplored. We combined intracellular recordings of membrane potential (V_m) of DGCs and local field potential recordings of the SWO in parietal cortex in anesthetized rats early during epileptogenesis [post-status epilepticus (SE) rats]. As expected, in control rats, the V_m of DGCs weakly and rarely oscillated in the SWO frequency range. In contrast, in post-SE rats, the V_m of DGCs displayed strong and long-lasting SWO. In

---

Significance Statement

Communication between cortex and hippocampus during sleep, orchestrated by the neocortical slow-wave oscillation (SWO), is important for memory consolidation. Whether this communication is affected in temporal lobe epilepsy (TLE), a disease with profound memory impairments, is not known. In control rats, dentate granule cells (DGCs), at the gate of the hippocampus, filter incoming information from the cortex. This relative independence of hippocampal neurons from SWO allows the replay of hippocampus-specific information independently from the neocortex. Here, using *in vivo* whole-cell patch-clamp recordings of DGCs and field recordings in the neocortex, we report an abnormally strong influence of neocortical SWO on the membrane potential and firing of DGCs in TLE rats. This could profoundly alter hippocampus–neocortex dialogue during sleep and associated cognitive functions.

these cells, clear UP and DOWN states, in phase with the neocortical SWO, led to a bimodal V_m distribution. In post-SE rats, the firing of DGCs was increased and more temporally modulated by the neocortical SWO. We conclude that UP/DOWN state dynamics dominate the V_m of DGCs and firing early during epileptogenesis. This abnormally strong neocortical influence on the dynamics of DGCs may profoundly modify the hippocampus–neocortex dialogue during sleep and associated cognitive functions.

Key words: dentate gyrus; epilepsy; in vivo whole-cell recordings; sleep; slow oscillation; UP/DOWN state

Introduction

During slow-wave sleep and anesthesia, neocortical networks are dominated by the slow oscillation [slow-wave oscillation (SWO), 0.1-2 Hz; Steriade et al., 1993, 2001; Cowan and Wilson, 1994]. At the cellular level, the membrane potential (V_m) of nearly all neocortical neurons synchronously alternates between epochs of steady depolarization (the UP state), associated with firing, and epochs of long-lasting hyperpolarization and quiescence (the DOWN state), leading to a bimodal distribution of their V_m (Timofeev et al., 2001; Volgushev et al., 2006; Rudolph et al., 2007; Chauvette et al., 2011). The SWO is not confined to neocortical networks and propagates to other subcortical (Wilson and Kawaguchi, 1996; Collins et al., 2001; Loewenstein et al., 2005; Mahon et al., 2006; Ros et al., 2009) and paleocortical (Isomura et al., 2006; Hahn et al., 2012) structures, where the V_m of principal cells also rhythmically alternates between UP and DOWN states. The SWO also propagates to the hippocampal formation (Isomura et al., 2006; Wolansky et al., 2006; Hahn et al., 2007). However, in contrast to cells in neocortical, subcortical, and paleocortical areas, the V_m of hippocampal principal neurons does not display rhythmic alternations between UP and DOWN phases for prolonged periods of time and lacks bimodality (unlike hippocampal interneurons, see Hahn et al., 2006). This suggests a lower impact of neocortical SWO on the V_m dynamics of hippocampal principal neurons than in other neocortical and subcortical structures. In line with this, the hippocampus can sometimes escape from the neocortical influence and generate specific activity patterns such

as sharp-wave ripples during the neocortical silent (DOWN) state (Isomura et al., 2006).

The aforementioned relative uncoupling of the hippocampus with neocortical SWO is in agreement with the gating function of the dentate gyrus, a major entry point to the hippocampus (Acsády and Kali, 2007). Indeed, dentate granule cells (DGCs) are relatively silent [e.g., firing no or few action potentials (APs) spontaneously] in awake, anesthetized, and sleeping animals (Jung and McNaughton, 1993; Leutgeb et al., 2007; Neunuebel and Knierim, 2012; Pernía-Andrade and Jonas, 2014; Diamantaki et al., 2016; Kowalski et al., 2016) and the proportion of active cells in a given environment is low (Chawla et al., 2005). In temporal lobe epilepsy (TLE), the dentate gyrus undergoes profound structural and functional network modifications (Dudek and Sutula, 2007). Several subtypes of inhibitory interneurons are lost (Sloviter, 1987; Houser and Esclapez, 1996), and the axons of DGCs (the mossy fibers) sprout to form a direct excitatory feedback circuit not present in controls (Tauck and Nadler, 1985; Represa et al., 1987; Scharfman et al., 2003; Epsztein et al., 2005). Altogether, these morphofunctional changes increase the excitability of DGCs (Artinian et al., 2011) and render the dentate "gate" more permissive to the propagation of neocortical pathological activities, such as epileptiform discharges (Nagao et al., 1996; Behr et al., 1998; Pathak et al., 2007; Bragin et al., 2012; Krook-Magnuson et al., 2015). These changes and associated gating abnormalities start to be observed very early during epileptogenesis (Wuarin and Dudek, 2001; Kobayashi and Buckmaster, 2003; Kobayashi et al., 2003; Pathak et al., 2007), and notably before the recording of the first spontaneous seizures (the latent period). Spatial memory deficits associated with the disease can already be observed at this early stage (Chauvière et al., 2009). Here we asked whether the impact of the physiological SWO on the dynamics of the V_m and firing of DGCs could be altered early during epileptogenesis.

To address this question, we combined whole-cell patch-clamp recordings of DGCs *in vivo* together with neocortical local field potentials (LFPs) recordings of the SWO in control and TLE rats under anesthesia during the latent phase of TLE [post-status epilepticus (SE) rats]. In contrast to control rats, the V_m of DGCs in post-SE rats showed strong UP/DOWN state dynamics that were time locked to the neocortical SWO. Furthermore, the firing of DGCs was increased and more strongly paced by the SWO in post-SE rats. We conclude that the processing of SWO, an important physiological pattern of neocortical activity during sleep, by DGCs is impaired early during epileptogenesis.

Correspondence should be addressed to Dr. Jérôme Epsztein, INMED/INSERM U901, Parc scientifique de Luminy, 163 route de Luminy, BP 13, 13273 Marseille cedex 09. E-mail: jerome.epsztein@inserm.fr.

Materials and Methods

Animals

All experiments were approved by the Institut National de la Santé et de la Recherche Médicale (INSERM) animal care and use committee and in accordance with the European community council directives (2010/63/UE). Data were obtained from male Wistar rats between the ages of postnatal day 27 (P27) to P43 (weight range, 100–130 g). We used the lithium/pilocarpine model of temporal lobe epilepsy with a ramp induction protocol. Rats were first injected with lithium chloride (3 mEq/kg). Fourteen to eighteen hours later, they were pretreated with methylscopolamine nitrate (1 mg/kg) to reduce the peripheral effects of pilocarpine. Thirty minutes after, they received a first low dose of pilocarpine (10 mg/kg). The same pilocarpine dose was repeatedly injected every 30 min until the behavioral manifestation of the first seizure was observed. The first seizure usually appeared after three to four doses of pilocarpine (30-40 mg/kg). This allowed us to take into account the individual differences in pilocarpine susceptibility between rats. One hour after the onset of status epilepticus, diazepam (8 mg/kg) was administered to stop the seizure. Recordings were performed 6-12 d after the status epilepticus. During this period, only interictal-like activities (ILAs), not seizures, could be recorded (mean frequency, 0.15 ± 0.07 Hz; ~9 ILAs/min; $n = 19$ rats).

Surgery

Animals were anesthetized with 1.5-2 g/kg urethane. The level of anesthesia was assessed using tail or foot pinching, body temperature, and recordings of the neocortical local field potentials. Body temperature was maintained at 37°C with a heating blanket (FHC). The animals were head fixed in a stereotaxic apparatus (SR-6, Narashige). A local analgesic (lidocaine) was applied as a gel on the ear bars to reduce pain during head fixation and was injected as a liquid below the skin before the first incision. An ophthalmic gel was applied to the eyes to prevent them from drying out during the surgery, and the eyes were covered with a piece of cardboard to protect them from the surgical light. The skull was exposed, and two small craniotomies (1.5 mm diameter) were drilled above the right hippocampus (−3.5 mm posterior to bregma; 2.5 mm lateral to bregma) to record in the dentate gyrus (~3 mm deep from brain surface) and above the parietal cortex (−4 mm posterior to bregma; 4 mm lateral to bregma) to record in the parietal cortex (1 mm deep from brain surface with an anteroposterior angle of 20°).

In vivo patch-clamp recordings

The V_m of DGCs was recorded in current-clamp mode using standard techniques for blind *in vivo* whole-cell recordings (Margrie et al., 2002). Borosilicate glass patch pipettes (resistance, 7–10 MΩ) were filled with a solution containing the following (in mM): 130 KMeSO4, 5 KCl, 5 NaCl, 10 HEPES-K, 2.5 MgATP, 0.3 NaGTP, 0.2 EGTA, and 0.1% biocytin, pH 7.25, adjusted with KOH. The V_m was amplified by an Axoclamp-2B Amplifier (Molecular Devices), low-pass filtered at 3 kHz, and digitized with a Digidata 1440A Digitizer (Molecular Devices) at 20 kHz. Only cells with overshooting APs, resting V_m less than −55 mV, and series resistance (R_s) <100 MΩ were kept for further analysis. The V_m was corrected for a 10 mV liquid junction potential.

LFPs and MUA recordings

LFPs and multiunit activity (MUA) were recorded from the parietal cortex and dentate granule cell layer using a glass electrode (~5 MΩ) filled with Ringer's solution (135 mM NaCl, 5.4 mM KCl, 1 mM MgCl$_2$, 1.8 mM CaCl$_2$, and 5 mM HEPES, pH adjusted to 7.2 with NaOH, and target osmolarity of 290 mmol/kg). LFPs and MUA were amplified 1000 times using a DAM80 amplifier (World Precision Instruments), bandpass filtered (0.1-3 kHz), digitized with a Digidata 1440A Digitizer (Molecular Devices), and sampled at 20 kHz. At the end of the recording, the pipette was submerged in a solution containing the red fluorescent dye 1,1'-dioctadecyl-3,3,3',3'-tetramethylindocarbocyanine perchlorate (DiI; Invitrogen), while the rat was still in the stereotaxic frame and reinserted at the recording depth for subsequent histological localization. Electrophysiological signals before and after DiI staining were similar.

Morphology of the recorded cells

At the end of the recordings, animals were injected with an overdose of urethane and transcardially perfused with PBS 1× solution followed by 4% paraformaldehyde. The next day, 100-μm-thick coronal slices were cut and processed with the avidin-biotin-CY3 method to visualize biocytin-filled neurons *post hoc*. The morphology of the recorded cells was reconstructed using Neurolucida software (MBF Bioscience).

Data analysis

Analyses were performed using custom-written programs in MATLAB (MathWorks), Origin (OriginLab), or Clampfit 10.4 (Molecular Devices).

Intrinsic intracellular properties

R_S values were not compensated for during the recording, but were calculated and compensated for off-line (Crochet and Petersen, 2006). To calculate R_S and membrane input resistance (R_N) values, we used voltage responses to multiple hyperpolarizing and depolarizing current steps (100 pA) injected shortly after breaking in. The voltage values used to calculate R_S (V_S) were found by exponentially fitting the voltage response (avoiding the first 2 ms during which the time constants resulting from pipette access resistance will dominate) to each current step. The exponential curve was then back-extrapolated to the start time of the step. The intersection of the extrapolated curve with the current step onset time gave V_S for each current step, which corresponds to the voltage drop across the R_S. R_S was then calculated as the slope of the linear fit of the I–V_S curve and used to correct V_m off-line by subtraction whenever current was injected through the patch pipette. After R_S off-line compensation, the R_N was calculated for each cell. The voltage values

used to determine R_N (V_N) were calculated for each step as the difference in V_m between the baseline (before the current pulse) and steady-state voltage (100 ms after the start of the current pulse). The R_N was also calculated not on a single step but by using all V_N values, as the slope of the corresponding $I–V_N$ curve. The membrane time constant was given by the time constant of the exponential fit of the V_N response to a 100 pA hyperpolarizing pulse. No holding current was injected during the recordings except when otherwise indicated. Resting membrane potential values were calculated as the mean of the Gaussian fit of V_m distribution using >30-s-long epochs. If the V_m distribution was best fitted by two Gaussian curves (bimodal cells), we used the voltage corresponding to the peak of the Gaussian curve fitting the lowest V_m hump values (the DOWN state). For all V_m analysis, the signal was detrended to remove ultraslow (<0.1 Hz) baseline fluctuations by low-pass filtering (0.1 Hz) then subtracting the low-pass-filtered data to the raw data. Threshold values were calculated using the first action potential in response to depolarizing steps of current as the voltage value at which the rate of depolarization (dV/dt) crossed 10 V/s.

Phase histograms

The times of intracellular APs were detected in high-pass-filtered (300 Hz) V_m as events higher than a predefined threshold. The times of MUA were determined in high-pass-filtered (1000 Hz) LFPs as events with amplitudes higher than five times the SD of the noise. The level of noise (and thus the detection threshold) was not significantly different between control and post-SE conditions ($p = 0.81$; $n = 6$ control rats, $n = 6$ post-SE rats). The phase of APs and MUA relative to the SWO cycle was derived from a Hilbert transformation of the LFP using the signal-processing toolbox in MATLAB. The peaks of the UP states are defined as 0° after the Hilbert transformation, and the troughs of the DOWN states are 180°. Phase modulation was evaluated by applying Rayleigh circular statistics (Fisher, 1993) .

Slow oscillatory epoch detection

Epochs of significant slow oscillations were detected using temporal spectral analysis of V_m in the SWO band (0.1-2 Hz; Fig. 1). Briefly, APs and hyperpolarizing steps used to probe the R_S during the recording were removed by linearly interpolating the signal. The time–frequency power spectrogram of V_m was computed using a 5 s sliding window advancing in steps of 0.2 s, and the time-varying power in the SWO frequency band (0.1-2 Hz) was extracted (Fig. 1A,B, bottom). For each control DGC, the value (Xi) corresponding to the highest 90% of all power values in the SWO frequency band was determined (Fig. 1C1). The average of all Xi values from control DGCs was then used as a unique threshold for SWO epoch detection in control and post-SE DGCs. The detection was performed on the time-varying power in the SWO frequency band (Fig. 1C2; see also Sales-Carbonell et al., 2013). A candidate SWO epoch should be above threshold for at least 4 s (e.g., approximately three oscillation cycles) to be considered as significant. For DGCs that spontaneously

fired in post-SE rats, the results were not significantly different if APs were not artificially removed from the data (power in SWO band: Student's t test, $p = 0.92$[mm]; duration of SWO epochs: Student's t test, $p = 0.89$[nn]; percentage of SWO: Mann–Whitney rank sum test, $p = 0.96$[oo]; $n = 8$).

V_m distribution

To determine whether the V_m of a DGC was unimodally distributed, the Hartigan dip test (Hartigan and Hartigan, 1985) was performed on the distribution of a >30 s low-pass-filtered (40 Hz) V_m epoch centered on epochs of significant slow oscillatory content using the Matlab routine by Nicholas Price (Monash University; http://www.nicprice.net/diptest/). Nonunimodal cells were classified as bimodal if their V_m distribution was best fitted by the sum of two Gaussian curves. Unimodal cells were further qualified as skewed if their skewness, measured with the "skewness" function of the MATLAB statistics toolbox, was >0.5.

LFP UP–DOWN state detection

UP and DOWN states were detected using the bimodal distribution of neocortical LFP values as previously described (Volgushev et al., 2006). Briefly, the level for DOWN state detection was set at the lower two-thirds of the distance between the peaks of the bimodal distribution of LFP values. The level for UP state detection was set at the higher two-thirds of the distance between the peaks of the bimodal distribution of LFP values (see Fig. 4A,B). States were defined as epochs above the threshold for UP states or below the threshold for DOWN states lasting >200 ms and were terminated when the threshold was crossed for >40 ms.

DOWN–UP transitions triggered V_m averages

The amplitude of V_m varies with time and across different cells. To compute the DOWN–UP transition (DUT)-triggered V_m averages, APs were removed from the signal by linear interpolation and subthreshold V_m values were converted into dimensionless units of z-score as follows: $Z(x) = (x − \text{mean}(x))/\text{SD}(x)$, where x is the V_m, mean is the average value of the variable, and SD is the standard deviation. Thus, the amplitude of V_m is represented in the units of z, thereby allowing easy comparison across different cells. The times of neocortical DOWN state endings were used as transition points from the DOWN to the UP state. The values of z-scored V_m, centered on the DOWN–UP transitions of neocortical SWO, were averaged across all detected neocortical DOWN–UP transitions.

Statistics

Statistical analyses were performed using SigmaStat (Systat Software), Statistica (Statsoft), and Prism (GraphPad) softwares (Table 1). For comparisons between groups with normal distribution and equal variance, the two-sample unpaired Student's t test was used. When data were not normally distributed or different variances were calculated between groups, the Mann–Whitney rank sum test was used. For comparisons before and after depolarization, the paired Student's t test was used when
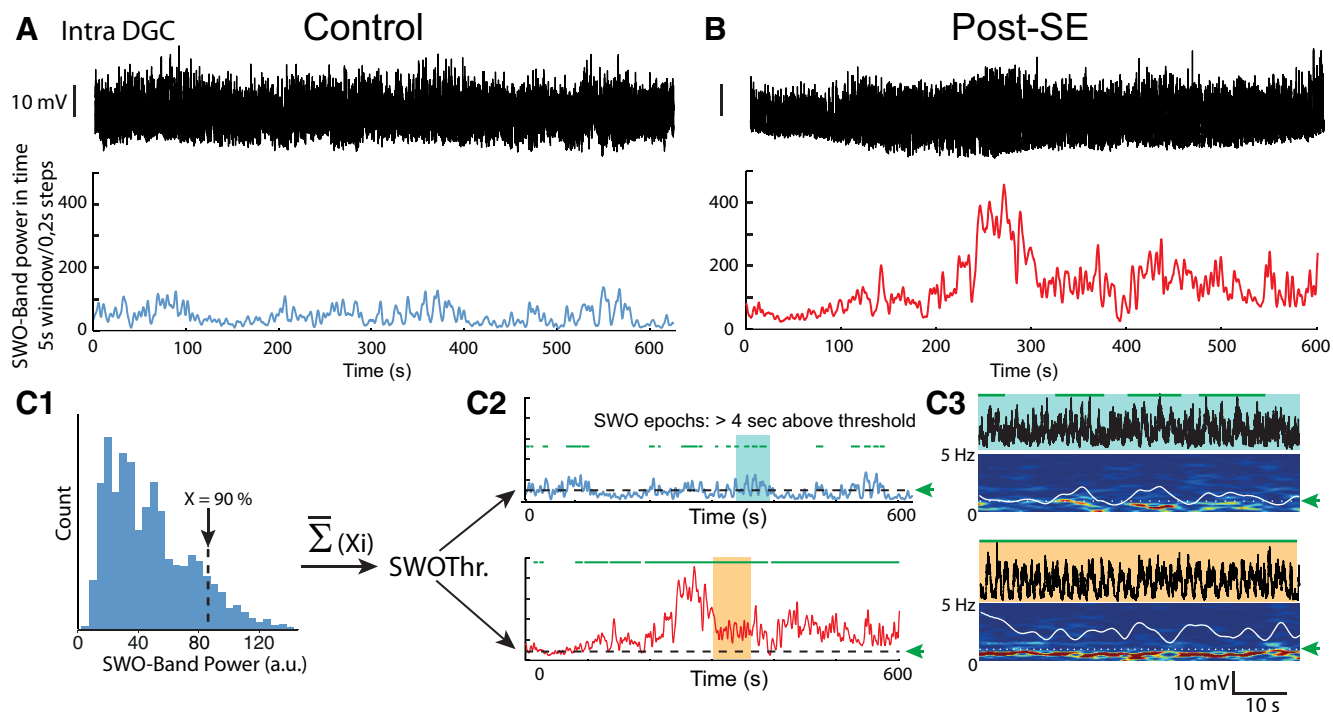
Figure 1. Method to compare the incidence and power of slow oscillations in the membrane potential of dentate granule cells from control and post-SE rats. ***A***, Top, V_m of a DGC from a control rat. The recording was bandpass filtered (0.1-40 Hz). Bottom, Time-varying power in the slow-frequency range (0.1-2 Hz) extracted from the time–frequency spectrogram of the V_m trace computed over a 5 s sliding window in 0.2 s steps. ***B***, Same as in ***A*** except that the cell from a post-SE rat was spontaneously firing (unlike the cell in ***A***), and spikes were digitally removed from the recording. Scale bar, as in ***A***. ***C1***, For each recording in controls, the 90th percentile highest value of the SWO band (0.1-2 Hz) power (*Xi*) was determined. The mean of all these values for control cells gives a unique threshold (SWOThr), which is then used to determine the SWO epochs in all DGCs from both control and post-SE rats. ***C2***, Example of the time-varying SWO power for the two recordings shown in ***A*** (top, blue) and ***B*** (bottom, red). Dashed lines correspond to the threshold for significant SWO epochs detection (green arrow). The epochs of high SWO power (green horizontal bars) are defined as epochs when the SWO power is above the threshold for >4 s. ***C3***, Illustration of detected SWO epochs corresponding to the light blue- and orange-shaded areas in ***C2***, Top, V_m traces. Bottom, Time–frequency spectrogram. Superimposed white lines represent the time-varying power values in the SWO band (0.1-2 Hz). Dashed white lines (green arrows) indicate the threshold used for SWO epochs detection (horizontal green bars above the traces).

values were normally distributed; otherwise, the Wilcoxon signed rank test was used. The level of significance was set at $p < 0.05$. If not stated otherwise, *n* refers to the number of cells. The power of statistical tests used was calculated using GraphPad StateMat software (Graph-Pad). Values are given as the mean ± SEM.

Pharmacological agents

All drugs (lithium chloride, scopolamine, pilocarpine, diazepam, and urethane) were diluted in NaCl 0.9% and administered intraperitoneally. Scopolamine methyl nitrate and pilocarpine hydrochloride were purchased from Sigma-Aldrich; diazepam was purchased from Roche; streptavidin conjugated to Cy3 was purchased from Jackson ImmunoResearch; and DiI was purchased from Life Technologies.

Results

UP and DOWN state dynamics of dentate granule cell membrane potential in post-SE rats

During slow-wave sleep and anesthesia, the V_m of neocortical cells rhythmically alternates between UP and DOWN states (Steriade et al., 1993, 2001; Cowan and Wilson, 1994). We first asked whether long-lasting epochs of UP/DOWN states could be detected in the V_m of DGCs from control and post-SE rats. We performed whole-cell patch-clamp recordings of DGCs *in vivo* in urethane-anesthetized control and post-SE rats (6–12 days after induction of a status epilepticus). Visual inspection of the V_m of DGCs from control rats did not reveal long-lasting epochs of UP/DOWN state modulation (Figs. 2A, 3A), as previously described (Isomura et al., 2006). In contrast, long-lasting epochs of UP/DOWN state modulation were observed in the V_m of the majority of DGCs from post-SE rats (Fig. 2B), interrupted by epochs of reduced slow oscillatory content (Fig. 3B). To automatically detect and compare epochs of slow oscillation in the V_m of DGCs, we developed a quantitative routine based on a single threshold set to the highest 90th percentile values of control DGCs' V_m power in the SWO band (0.1-2 Hz; see also Sales-Carbonell et al., 2013; see Experimental procedure/Data analysis/Slow oscillatory epoch detection; Fig. 1C). Epochs of significant SWO power were detected in 6 of 10 DGCs from control rats. The duration of each SWO epoch

Table 1: Statistical table

	Data structure	Type of test	Power or 25-75% confidence intervals
a	Normality test: passed ($p = 0.12$) Equal variance test: failed ($p < 0.05$)	Mann–Whitney rank sum test	25-75% control: 7–10.5; post-SE: 12.5–64.6
b	Normality test: passed ($p = 0.16$) Equal variance test: passed ($p = 0.36$)	Two-sample Student's t test	0.99
c	Normality test: passed ($p = 0.61$) Equal variance test: failed ($p < 0.05$)	Mann–Whitney rank sum test	25-75% control: 7–45.3; post-SE: 54.6–109
d	Normality test: passed ($p = 0,18$) Equal variance test: passed ($p = 0.44$)	Two-sample Student's t test	0.88
e	Normality test: passed ($p = 0.36$) Equal variance test: failed ($p < 0.05$)	Mann–Whitney rank sum test	25-75% control: -0.14 to -0.08; post-SE: -0.36 to -0.15
f	Normality test: passed ($p = 0.59$) Equal variance test: passed ($p = 0.80$)	Two-sample Student's t test	0.30
g	Normality test: passed ($p = 0.32$) Equal variance test: failed ($p < 0.05$)	Mann–Whitney rank sum test	25-75% control: -43.5 to -39.0; post-SE: -39.9 to -37.4
h	Normality test: passed ($p = 0.056$) Equal variance test: passed ($p = 0.82$)	Two-sample Student's t test	0.20
i	Normality test: passed ($p = 0.37$) Equal variance test: passed ($p = 0.73$)	Two-sample Student's t test	0.20
j	Normality test: passed ($p = 0.49$) Equal variance test: passed ($p = 0.36$)	Two-sample Student's t test	0.60
k	Normality test: failed ($p < 0.05$)	Mann–Whitney rank sum test	25-75% control: 7.75–10.4; post-SE: 9.4–16.8
l	Normality test: passed ($p = 0.13$) Equal variance test: passed ($p = 0.26$)	Two-sample Student's t test	0.99
m	Normality test: passed ($p = 0.44$) Equal variance test: passed ($p = 0.18$)	Two-sample Student's t test	0.70
n	Normality test: passed ($p = 0.054$) Equal variance test: passed ($p = 0.22$)	Two-sample Student's t test	0.52
o	Normality test: passed ($p = 0.10$) Equal variance test: passed ($p = 0.56$)	Two-sample Student's t test	0.30
p	Normality test: passed ($p = 0.25$) Equal variance test: passed ($p = 0.52$)	Two-sample Student's t test	0.90
q	Normality test: passed ($p = 0.12$)	One-sample Student's t test	0.99
r	Normality test: failed ($p = 0.008$)	One-sample Wilcoxon signed rank test	25–75%: post-SE: 0.37–0.55
s	Normality test: passed ($p = 0.85$) Equal variance test: passed ($p = 0.44$)	Two-sample Student's t test	0.99
t	Normality test: failed ($p < 0.05$)	Mann–Whitney rank sum test	25–75% control: 0–0; post-SE: 0.02–0.76
u	Normality test: failed ($p < 0.05$)	Mann–Whitney rank sum test	25–75% control: 0–0; post-SE: 0.32–17.9
v	Normality test: failed ($p < 0.05$)	Mann–Whitney rank sum test	25–75% control: 1.15–1.27; post-SE: 1.17–1.33
w	Normality test: failed ($p < 0.05$)	Mann–Whitney rank sum test	25–75% control: 0–0; control depolarization: 0.16–0.43
x	Normality test: failed ($p < 0.05$)	Mann–Whitney rank sum test	25–75% post-SE: 0.02–0.76; control depolarization: 0.16–0.43
y	Normality test: passed ($p = 0.099$)	Paired t test	0.94
z	Normality test: passed ($p = 0.645$) Equal variance test: passed ($p = 0.709$)	Two-sample Student's t test	0.99
aa	Normality test: passed ($p = 0.64$) Equal variance test: passed ($p = 0.602$)	Two-sample Student's t test	0.99
bb	Normality test: passed ($p = 0.48$) Equal variance test: failed ($p < 0.05$)	Mann–Whitney rank sum test	25–75% control: 0.68–2.62; post-SE: 2.30–13.1
cc	Normality test: passed ($p = 0.73$) Equal variance test: failed ($p < 0.05$)	Mann–Whitney rank sum test	25–75% control: 0.21–0.53; post-SE: 0.15–0.23
dd	Normality test: failed ($p < 0.05$)	Mann–Whitney rank sum test	25–75% control: 97.8–193; post-SE: 66.7–229
ee	Normality test: passed ($p = 0.61$) Equal variance test: failed ($p < 0.05$)	Mann–Whitney rank sum test	25–75% control: 71.1–74.8; post-SE: 55.6–69.0
ff	Normality test: failed ($p < 0.05$)	Mann–Whitney rank sum test	25–75% control: 3.27–8.72; post-SE: 3.9–8.2
gg	Normality test: passed ($p = 0.43$) Equal variance test: passed ($p = 0.25$)	Two-sample Student's t test	0.99
hh	Normality test: passed ($p = 0.79$) Equal variance test: passed ($p = 0.24$)	Two-sample Student's t test	0.95
ii	Normality test: passed ($p = 0.70$) Equal variance test: passed ($p = 0.42$)	Two-sample Student's t test	0.99

(Continued)

Table 1: Continued

	Data structure	Type of test	Power or 25-75% confidence intervals
jj	Normality test: passed ($p = 0.23$)	Paired t test	0.99
kk	Normality test: failed ($p < 0.05$)	Wilcoxon signed rank test	25–75% control: 7.04–10.46; control depolarization: 7.62–14.4
ll	Normality test: passed ($p = 0.56$)	Paired t test	0.98
mm	Normality test: passed ($p = 0.22$) Equal variance test: passed ($p = 0.92$)	Two-sample Student's t test	0.80
nn	Normality test: passed ($p = 0.14$) Equal variance test: passed ($p = 0.83$)	Two-sample Student's t test	0.40
oo	Normality test: failed ($p < 0.05$)	Mann–Whitney rank sum test	25–75% post-SE no spike: 48.5–82.9; post-SE with spikes: 48.2–82.7
pp	Normality test: failed ($p < 0.05$)	Mann–Whitney rank sum test	25–75% post-SE: 0.32–17.9; control depolarization: 7.61–12.9

was short (8.44 ± 1.26 s; range, 4.8-13.6 s; $n = 6$; Figs. 2A, 3A,C), and together they represented a small proportion of overall recording time (12.8 ± 4.90%; mean total duration of SWO per recording, 75 ± 28 s; mean recording time, 598 ± 25 s; $n = 10$; Fig. 3D). In contrast, epochs of strong SWO power could be detected in all DGCs from post-SE rats ($n = 8$ of 8). The duration of each SWO epoch was on average much longer than in the control condition (38.8 ± 11.3 s; range, 5.36–93.6 s; $n = 8$; Mann–Whitney rank sum test, $p = 0.029$[a]; Figs. 2B, 3B,C). Added up, these epochs represented a larger proportion of the total recording time (62.8 ± 10.2%; Student's t test, $p = 0.0006$[b]; mean total duration of SWO per recording, 360 ± 66 s; mean recording time, 584 ± 49 s; $n = 8$; Fig. 3D). Over all recorded cells and recording time, the SWO band power of the Vm of DGCs was approximately three times higher in the post-SE versus the control condition (Mann–Whitney rank sum test, $p = 0.004$[c]; Fig. 3E). Power spectral analysis of the V_m of DGCs centered on these epochs revealed a high peak at ~0.8 Hz in post-SE rats, while a smaller peak (Student's t test, $p = 0.004$[d]) was observed at a lower frequency (~0.4 Hz) in controls (Fig. 2C,D). Autocorrelograms of the V_m of DGCs during these epochs revealed a higher rhythmicity in the post-SE versus the control condition with larger negative peaks (minimum amplitude at trough, −0.26 vs −0.11; Mann–Whitney rank sum test, $p = 0.037$[e]; $n = 8$ and 10 cells, respectively; Fig. 2E,F) and second positive peaks in the post-SE condition, which were not present in controls. We conclude that the V_m of DGCs in post-SE rats strongly oscillates in the slow-frequency range for prolonged periods of time, unlike what is observed in controls.

We next wondered whether V_m dynamics were similar during SWO epochs in DGCs from control and post-SE rats. Analysis of the V_m distribution revealed in a majority of DGCs from post-SE rats a nonunimodal but bimodal distribution, a signature of strong UP/DOWN state dynamics (Hartigan's dip test of unimodality, $p = 0.017 ± 0.008$; see Materials and Methods; Fig. 2B3; $n = 5$ of 8 cells). In the remaining cells, the V_m distribution was unimodal, either symmetrical ($n = 1$) or skewed ($n = 2$; see Materials and Methods). In DGCs from control rats, however, the distribution was always unimodal (Hartigan's dip test of unimodality, $p = 0.80 ± 0.25$; $n = 10$; Isomura et al., 2006; Hahn et al., 2007), either skewed ($n = 6$) or

symmetrical ($n = 4$; Fig. 2A3). These differences in V_m dynamics between DGCs from control and post-SE rats were not due to major differences in their intrinsic properties (Table 2).

We conclude that SWO and UP/DOWN state behavior are major components of V_m dynamics in DGCs from post-SE rats, unlike what is observed in DGCs from control rats.

Temporal relationship between the membrane potential of dentate granule cells and the neocortical slow oscillation in control and post-SE rats

Before investigating the temporal relationship between neocortical SWO and the V_m of DGCs, we first wondered whether neocortical SWO was modified during the latent period in TLE (Fig. 4). LFP recordings in the parietal cortex (which projects to the medial entorhinal cortex; Burwell and Amaral, 1998) revealed no change in SWO power (Student's t test, $p = 0.40$[l]) and rhythmicity (Student's t test, $p = 0.71$[m]) between control ($n = 10$) and post-SE ($n = 10$) rats (Fig. 4A,C–F). The only difference was a small but significant increase in UP phase duration (control rats, 374 ± 16 ms; post-SE rats, 450 ± 28 ms; $n = 10$; Student's t test, $p = 0.03$[n]; Fig. 4G), while DOWN phase duration was not changed (Student's t test, $p = 0.74$[o]; Fig. 4H). However, this difference did not result in a significant change of the parietal cortex SWO frequency (control rats, 0.75 ± 0.07 Hz; post-SE rats, 0.74 ± 0.06 Hz; $n = 10$; Student's t test, $p = 0.88$[p]; Fig. 4D,F).

We next looked for a temporal coupling between the neocortical SWO in the parietal cortex and the V_m of DGCs. Cross-correlation between the V_m of DGCs and LFPs of parietal cortex was small and peaks were highly temporally jittered for DGCs recorded in control rats ($r = 0.05 ± 0.03$; one-sample Student's t test, $p = 0.15$[q]; $n = 10$; Fig. 5A,C,E). In contrast, the correlation was high and highly significant in post-SE rats ($r = 0.45 ± 0.04$; one-sample Wilcoxon signed rank test, $p = 0.008$[r]; $n = 8$; Fig. 5B,D,E) with a fixed delay (166 ± 33.7 ms; $n = 8$). To better characterize the temporal relationship between activities recorded in the two structures we used the DOWN to UP transitions (DUT) of the neocortical SWO (see Materials and Methods) as a temporal reference to examine the V_m of DGCs (DUT-triggered V_m; Fig. 5F–H; Isomura et al., 2006; Hahn et al., 2007). Examination of
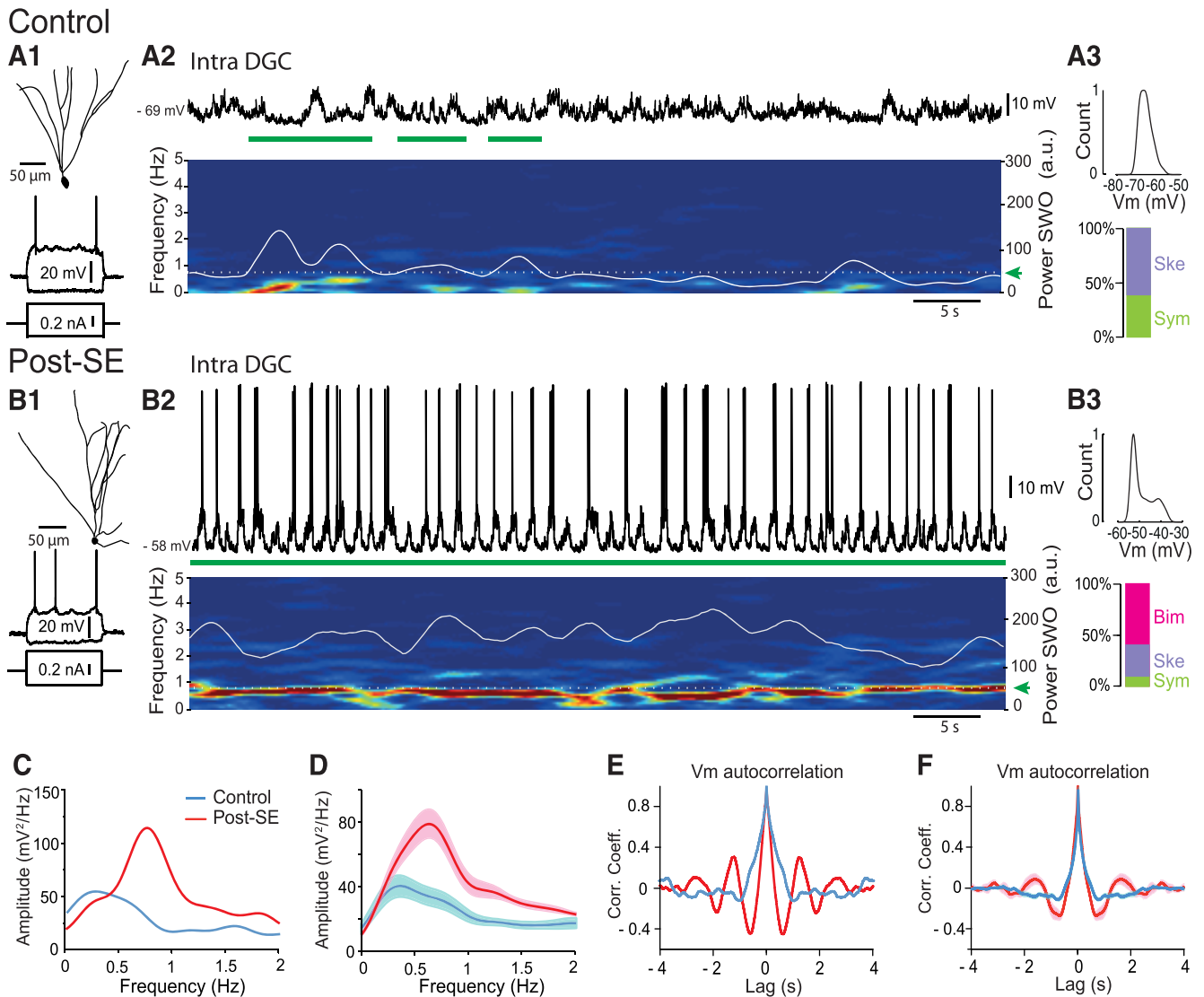
Figure 2. Increased slow-oscillatory UP/DOWN state dynamics of the membrane potential of dentate granule cells in post-SE rats. **A1**, Neurolucida reconstruction of the morphology of a recorded dentate granule cell from a control rat (top) and voltage responses to intracellularly injected depolarizing and hyperpolarizing current pulses (500 ms duration, bottom). **A2**, Top, V_m of the cell illustrated in **A1** during a 60 s recording. Bottom, Time–frequency power spectrogram (5 s sliding window, 0.2 s steps) corresponding to the top trace. Superimposed white line represents the time-varying power values in the SWO frequency range (0.1-2 Hz). Dashed white line (green arrow) indicates the SWO detection threshold used to detect SWO epochs (horizontal green bars). **A3**, Top, Distribution of V_m values for the trace shown in **A2**, Bottom, Relative proportion of DGCs according to the distribution of their V_m (Ske., skewed; Sym., symmetric; $n = 10$). **B**, Same as in **A** for the post-SE condition. Note the presence of a continuous band in the slow-frequency range (~0.8 Hz), and bimodal distribution of the V_m in the DGC from post-SE, but not control, rat (Bim., bimodal). **C**, Power spectrum of the traces shown in **A** (blue) and **B** (red). **D**, Average power spectrum for all recorded DGCs in control (blue line; $n = 10$) and post-SE (red line; $n = 8$). **E**, Autocorrelogram of the traces shown in **A** (blue) and **B** (red). **F**, Mean autocorrelogram for all recorded DGCs in control (blue line; $n = 10$) and post-SE (red line; $n = 8$). Light blue- and pink-shaded areas correspond to ±SEM.

DUT-triggered averaged V_m values showed a positive bump at a fixed latency following neocortical DUT in all DGCs in post-SE rats (Fig. 5G). However, the individual responses in control rats were less consistent, often showing an absence of a clear bump after the neocortical DOWN–UP transition and in one case even a downward shift (Fig. 5F). In line with the results from individual cells, in post-SE rats, the mean DUT-

triggered V_m average showed a clear bump with a peak at 317 ms following neocortical DUTs (Fig. 5H; $n = 3543$ DUTs in 8 cells), while no positive bump was observed in controls (Fig. 5H; $n = 4864$ DUTs in 10 cells; Student's t test, $p = 0.0005^s$ vs post-SE at peak).

We conclude that long-lasting UP/DOWN dynamics of the V_m of DGCs in post-SE rats is temporally locked to the neocortical SWO.
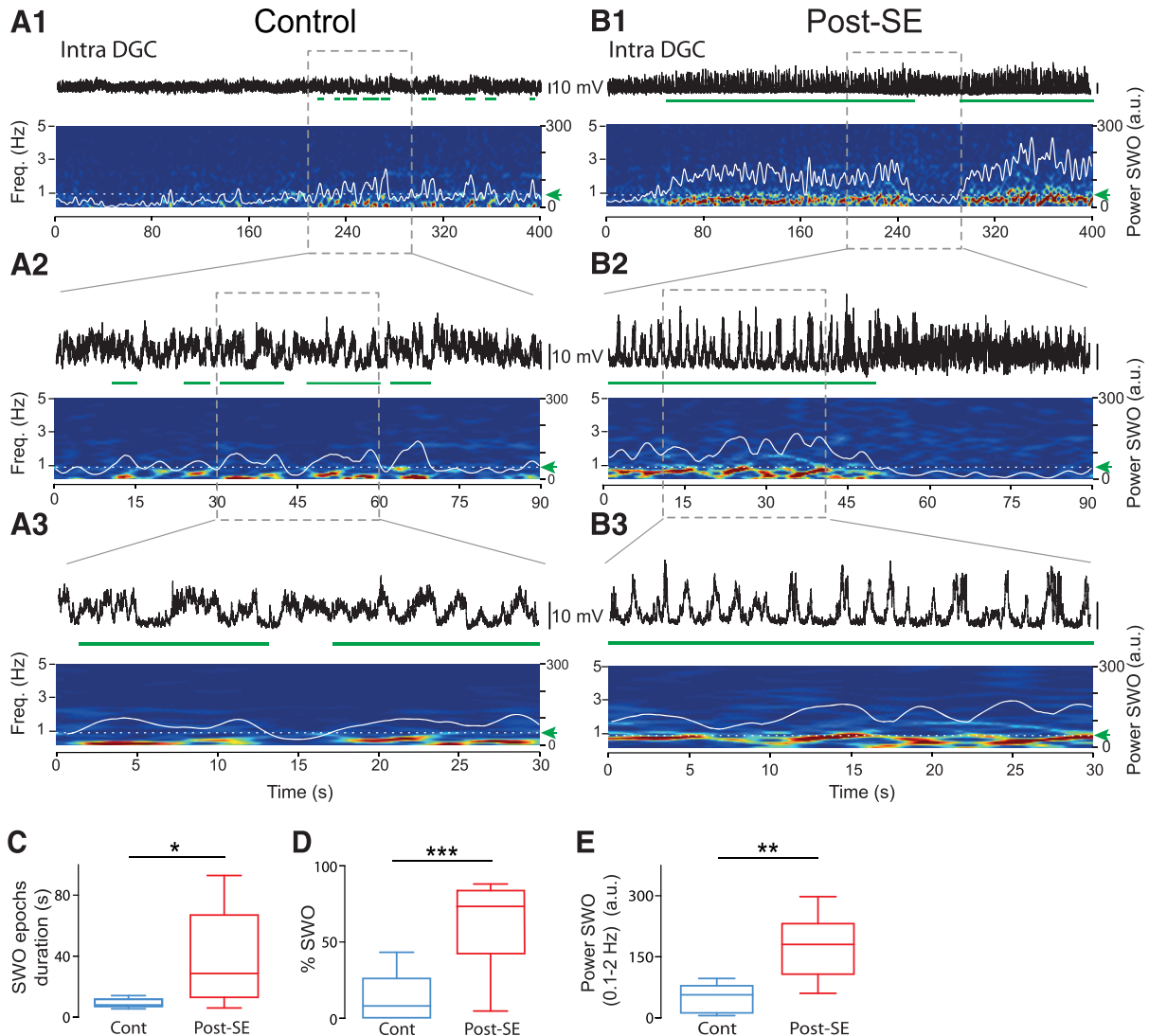
Figure 3. Increased slow-oscillatory epochs in the membrane potential of dentate granule cells in post-SE rats. ***A***, ***B***, Examples of detected SWO epochs in the membrane potential of dentate granule cells from a control rat (***A***) and a post-SE rat (***B***; spikes digitally removed). In each panel, the V_m (top), time–frequency power spectrogram (bottom) and time-varying power in the SWO band (0.1-2 Hz; superimposed white line) are represented at low (1) intermediate (2), and high (3) temporal resolution. In all cases, green horizontal bars below the trace highlight detected SWO epochs (Scale bars in ***B***, same as in ***A***). ***C***, Box plots of the duration of single SWO epochs detected in the V_m of DGCs in control ($n = 6$) and post-SE ($n = 8$) conditions. ***D***, Box plots of the percentage of recording time with significant oscillations in the SWO frequency range in the V_m of DGCs in control ($n = 10$) and post-SE ($n = 8$) rats. ***E***, Box plots of the power in the SWO frequency range averaged over all recorded cells and recording times in the V_m of DGCs in control ($n = 10$) and post-SE ($n = 8$) rats. For these and subsequent box plots, the box extends from the 25th to 75th percentile. The line in the middle of the box is the median. The whiskers go down to the smallest value and up to the largest. $*p < 0.05$; $**p < 0.01$; $***p < 0.001$.

Modulation of the firing of dentate granule cells by the neocortical slow oscillation in control and post-SE rats

We next aimed at determining whether the change in the dynamics of the V_m of DGCs observed in post-SE rats had any impact on their firing. We did this both at the single-cell level using intracellular recordings of the spiking activity of DGCs (Fig. 6) and at the network level using extracellular recordings of MUA in the dentate granule cell layer (see Fig. 8).

The V_m of DGCs from control rats was hyperpolarized (-79.1 ± 2.47 mV; $n = 10$), and most of them (80%) were silent (i.e. not firing any spontaneous action potential) during the recording time (mean recording time of silent cells, 892 ± 225 s; range, 410–2273 s; $n = 8$). The mean firing rate was low (active cells: 0.14 ± 0.08 Hz, $n = 2$; all cells: 0.03 ± 0.02 Hz, $n = 10$). Accordingly, few neocortical UP phases were associated with the firing of intracellularly recorded DGCs in controls (mean, $1.97 \pm 1.81\%$; $n = 10$). In contrast, 75% of DGCs were sponta-

Table 2: Dentate granule cells intrinsic properties

	Control (n = 10)	Post-SE (n = 8)	p value
Resting membrane potential (mV)	−79.1 ± 2.47	−74.8 ± 3.00	0.28[f]
Action potential threshold (mV)	−51.7 ± 1.10	−48.8 ± 0.48	0.08[g]
Action potential amplitude (mV)	55.9 ± 4.22	48.7 ± 5.44	0.30[h]
Action potential half-width (ms)	0.77 ± 0.03	0.80 ± 0.03	0.47[i]
Membrane input resistance (MΩ)	81.4 ± 8.27	94.9 ± 11.7	0.35[j]
Membrane time constant (ms)	11.2 ± 2.96	13.1 ± 1.88	0.06[k]

Values are represented as the mean ± SEM. All statistical comparisons were performed using the Student's t test, except for Action potential threshold and Membrane time constant, where the Mann–Whitney rank sum test was used.

neously firing in post-SE rats (Fig. 6A,B; active cells: 0.84 ± 0.47 Hz, $n = 6$; all cells: 0.63 ± 0.37 Hz, $n = 8$; Mann–Whitney rank sum test, $p = 0.029^t$ for all cells), and the number of neocortical UP phase associated with the firing of DGCs was significantly higher (Fig. 6C; mean = 13.4 ± 6.81%; Mann–Whitney rank sum test, $p = 0.045^u$; $n = 8$). However, when spiking was observed during a neocortical UP phase, the mean number of spikes was
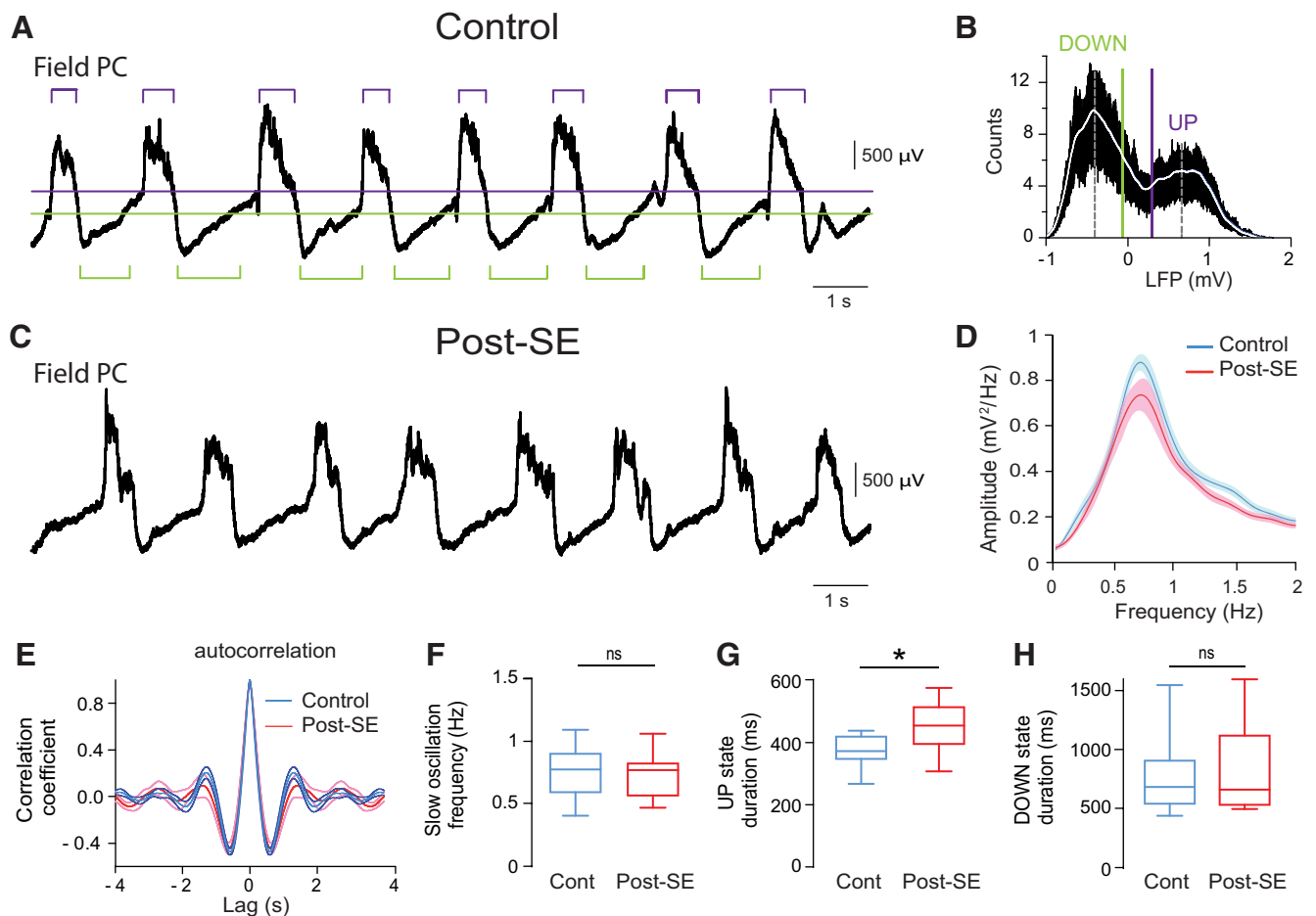

Figure 4. Comparing neocortical local field potential slow oscillations between control and post-SE rats. **A**, Example LFP recorded in the parietal cortex in a control rat, with the threshold levels used to detect UP or DOWN states indicated by horizontal bars (green, DOWN state; purple, UP state). **B**, Histogram of the distribution of LFP values for the trace shown in **A**. The level for DOWN state detection (green vertical line) was set at the lower two-thirds of the distance between the peaks of the bimodal distribution of LFP values. The level for UP state detection (purple vertical line) was set at the higher two-thirds of the distance between the peaks of the bimodal distribution of LFP values. **C**, Example LFP recorded in the parietal cortex from a post-SE rat. **D**, Mean power spectrum of the LFPs recorded in the parietal cortex. Control ($n = 10$) and post-SE ($n = 10$) in **D–H**. **E**, Average autocorrelogram of LFPs in control (blue line) and post-SE (red line) conditions with a nonsignificant difference at the negative peaks. **F**, Box plots of the frequency of the neocortical SWO in control and post-SE rats. **G**, Box plots of neocortical UP state duration in control and post-SE rats. **H**, Box plots of neocortical DOWN state duration in control and post-SE rats. Light blue- and pink-shaded areas in **D** and thinner lines in **E** indicate SEM. ns, $p > 0.05$; ∗$p < 0.05$. For description of box plots, see the legend of Figure 3.
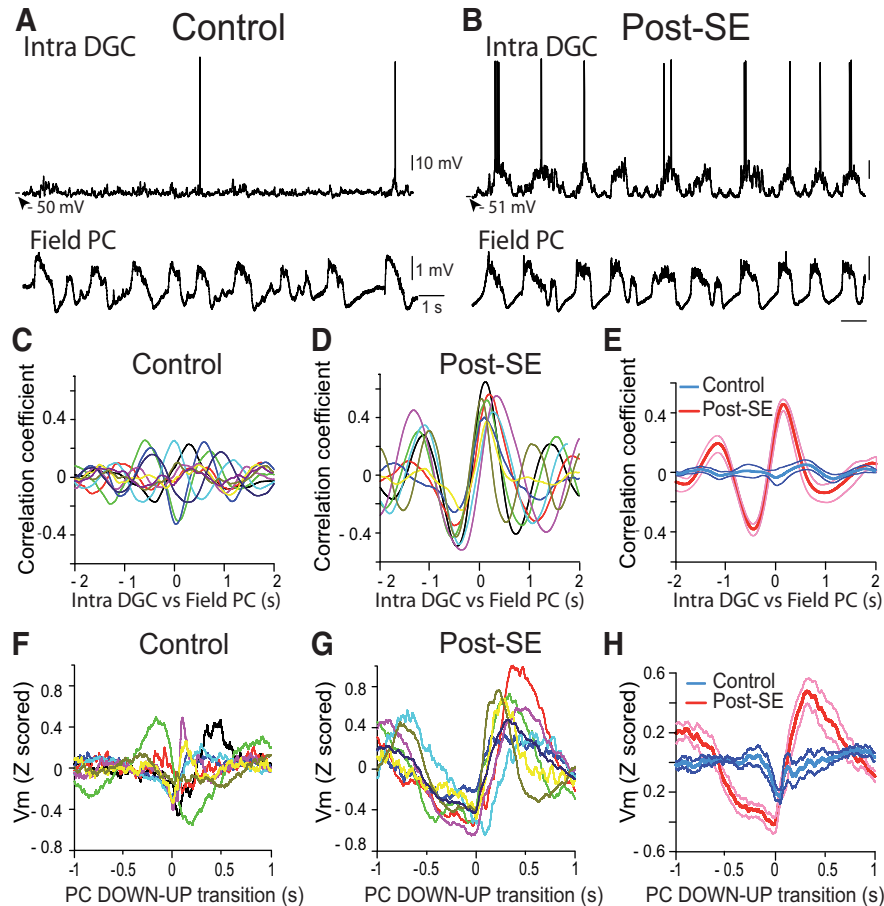
Figure 5. Strong temporal correlation between the membrane potential of dentate granule cells and the parietal cortex local field potential in post-SE rats, but not in control rats. ***A***, V_m of a DGC from a control rat (top) and simultaneously recorded LFP in the parietal cortex (bottom). ***B***, Same as in ***A*** for a DGC from a post-SE rat. Scale bars are as in ***A***. ***C***, V_m vs LFP cross-correlograms for all individual DCGs from control rats ($n = 10$). ***D***, Same as in ***C*** for DGCs from post-SE rats ($n = 8$). ***E***, Average V_m vs LFP cross-correlogram of all DGCs recorded in control rats (blue line, $n = 10$) and post-SE rats (red line, $n = 8$). ***F***, DOWN–UP transition-triggered V_m for all individual DGCs from control rats ($n = 10$). ***G***, Same as in ***F*** for DGCs from post-SE rats ($n = 8$). ***H***, Average DOWN–UP transition-triggered V_m for DGCs recorded in control rats (blue line, $n = 10$) and post-SE rats (red line, $n = 8$). Thinner lines in ***E*** and ***H*** represent ±SEM.

not significantly higher in the post-SE versus the control condition (post-SE: 1.36 ± 0.16 spikes per neocortical UP phase, $n = 524$ UP phases with spikes in eight cells; control: 1.21 ± 0.06 spikes per neocortical UP phase, $n = 86$ UP phases with spikes in two cells; Mann–Whitney rank sum test, $p = 0.64^y$). In post-SE DGCs, spikes were strongly and precisely modulated by the neocortical SWO (mean length of Rayleigh vector, 0.72 ± 0.06; mean phase dispersion, 41.2 ± 4.44 degrees; $n = 6$; Fig. 6D). We conclude that the firing of DGCs in post-SE rats is increased and highly modulated by the neocortical SWO.

Because DGCs from control rats rarely fire or fire at a very low rate, it is difficult to determine whether their firing can be modulated by the neocortical SWO. To circumvent this problem, we artificially depolarized control cells to induce a firing rate comparable to that observed in DGCs from post-SE rats (mean Vm after depolarization, -56.5 ± 2.55 mV; $n = 8$ of 8 cells firing; mean firing rate, 0.29 ± 0.06 Hz; Mann–Whitney rank sum test, $p = 0.02^w$ vs

control rats; $p = 0.72^x$ vs post-SE rats; $n = 10$ control DGCs; $n = 8$ control DGCs depolarized; $n = 8$ post-SE DGCs; Fig. 6E,F). Under depolarization, the number of neocortical UP phases associated with intracellular spiking was also significantly increased (paired Student's t test, $p = 0.004^y$ before vs after depolarization; Fig. 6G; Mann–Whitney rank sum test, $p = 0.64^{pp}$ vs post-SE; $n = 8$). However, in this condition, spikes were significantly less strongly and less precisely modulated by the neocortical SWO than spikes from DGCs in post-SE rats (mean length of Rayleigh vector, 0.29 ± 0.07; Student's t test, $p = 0.0007^z$ vs post-SE; mean phase dispersion, $67.7 \pm 3.47°$; Student's t test, $p = 0.0005^{aa}$ vs post-SE; $n = 8$ control DGCs depolarized; $n = 6$ post-SE DGCs; compare Fig. 6D,H). Furthermore, the modulation of the V_m of control DGCs by the neocortical SWO was not significantly increased after depolarization (Fig. 7). Thus, when the spiking of control DGCs is artificially increased through direct depolarization, the modulation of their firing
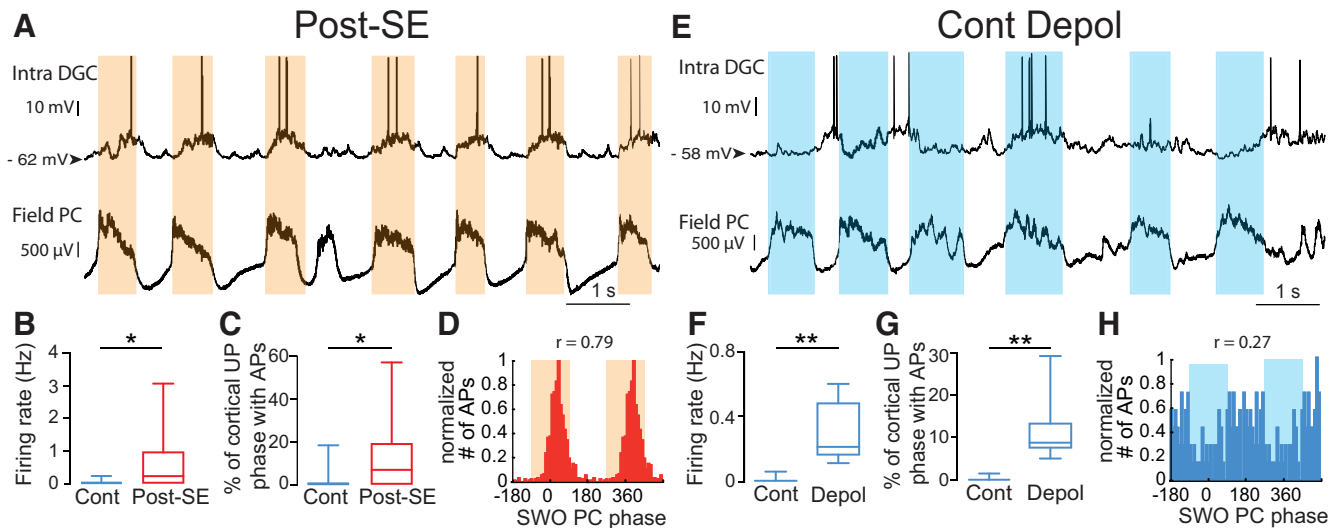
Figure 6. Modulation of the action potentials of dentate granule cells by the neocortical slow oscillation in post-SE and control rats. *A*, *E*, Membrane potential of a DGC (top) recorded in a post-SE rat (*A*) or a control rat after depolarization to induce spontaneous firing (*E*) and simultaneously recorded local field potentials in the parietal cortex (bottom). *B*, Box plots of the firing frequency of intracellularly recorded DGCs from control rats (with no added depolarization; $n = 10$) and post-SE rats ($n = 8$). *C*, Box plots of the percentage of neocortical UP phases associated with at least one AP in the control condition (with no added depolarization; $n = 10$) and post-SE condition ($n = 8$). *D*, Phase distribution histogram of APs recorded in the DGC shown in *A* in reference to SWO phase in the parietal cortex. The orange-shaded area depicts the UP phase of SWO simultaneously recorded in the parietal cortex. *F*, Same as in *B* for DGCs from control rats before and after depolarization to induce spontaneous firing ($n = 8$). *G*, Same as in *C* for DGCs from control rats before and after depolarization to induce spontaneous firing ($n = 8$). *H*, Same as in *D* for the cell illustrated in *E*. *$p < 0.05$; **$p < 0.01$. For a description of box plots, see the legend of Figure 3.

by the neocortical SWO is much weaker and less precise than that of DGCs from post-SE rats. Accordingly, their V_m does not show strong SWO modulation.

To see whether the increased spiking rate and SWO modulation of DGCs from post-SE rats could be observed at the network level, we next recorded MUA in the dentate granule cell layer of control and post-SE rats. MUA was significantly increased in post-SE ($n = 17$) versus control ($n = 7$) rats (Fig. 8*A,B,G*; 7.80 ± 1.44 Hz in post-SE rats; 1.61 ± 0.41 Hz in control rats; Mann–Whitney rank sum test, $p = 0.01$[bb]). We compared the strength of the modulation of MUA by the neocortical SWO in control and post-SE conditions (Fig. 8*C,E*). MUA in post-SE rats was more strongly modulated by the neocortical SWO (Fig. 8*H*; mean length of Rayleigh vector, 0.39 ± 0.04 in post-SE rats vs 0.19 ± 0.03 in control rats; Mann–Whitney rank sum test, $p = 0.031$[cc]), the mean phase at which MUA occurred was not different (Fig. 8*I*; Mann–Whitney rank sum test, $p = 0.95$[dd]), but the dispersion around the mean phase was significantly smaller in post-SE rats (Fig. 8*J*; mean phase dispersion, 61.6 ± 2.26° in post-SE rats vs 72.7 ± 1.47° in controls; Mann–Whitney rank sum test, $p = 0.01$[ee]). In sharp contrast, MUA recorded in the parietal cortex was not significantly increased in post-SE ($n = 17$) versus control ($n = 14$) rats (Mann–Whitney rank sum test, $p = 0.86$[ff]; Fig. 9*A–C*), nor was the strength of MUA modulation by the SWO (Student's t test, $p = 0.96$[gg]; Figs. 8*D,F*, 9*D*), the mean phase (Student's t test $p = 0.48$[hh]; Fig. 9*E*) or the phase dispersion around the mean (Student's t test, $p = 0.86$[ii]; Fig. 9*F*).

Discussion

In the present study, we investigated whether the impact of the neocortical SWO on DGCs, at the gate of the hippocampus, could be altered in an animal model of TLE. In line with this hypothesis, while the V_m of control DGCs weakly oscillated in the SWO frequency range for short periods of time, the V_m of most DGCs from post-SE rats showed strong UP/DOWN state dynamics for extended periods, time locked to neocortical SWO. Furthermore, the firing of DGCs was increased and strongly modulated by the neocortical SWO in post-SE rats, but not in control rats. Altogether, these results point to a major alteration in the processing of SWO, an important physiological pattern of activity, by DGCs during the early phase of TLE.

Possible mechanisms of the switch to strong UP/DOWN state V_m dynamics in post-SE DGCs

A great deal of experimental and computational work has been conducted to understand the mechanisms leading to neocortical SWO and associated neuronal UP/DOWN state dynamics in the cortex (Timofeev et al., 2000; Bazhenov et al., 2002; Compte et al., 2003; Cossart et al., 2003; Shu et al., 2003; Haider et al., 2006; Holcman and Tsodyks, 2006; Rudolph et al., 2007; Chauvette et al., 2010). SWO has been proposed to result either from synaptic or intrinsic mechanisms. In the synaptic hypothesis, stochastic EPSPs could summate during the DOWN state and reach the activation threshold of intrinsic conductances, such as I_{NaP}, initiating the UP state (Timofeev et al., 2000; Chauvette et al., 2010). Alternatively, SWO
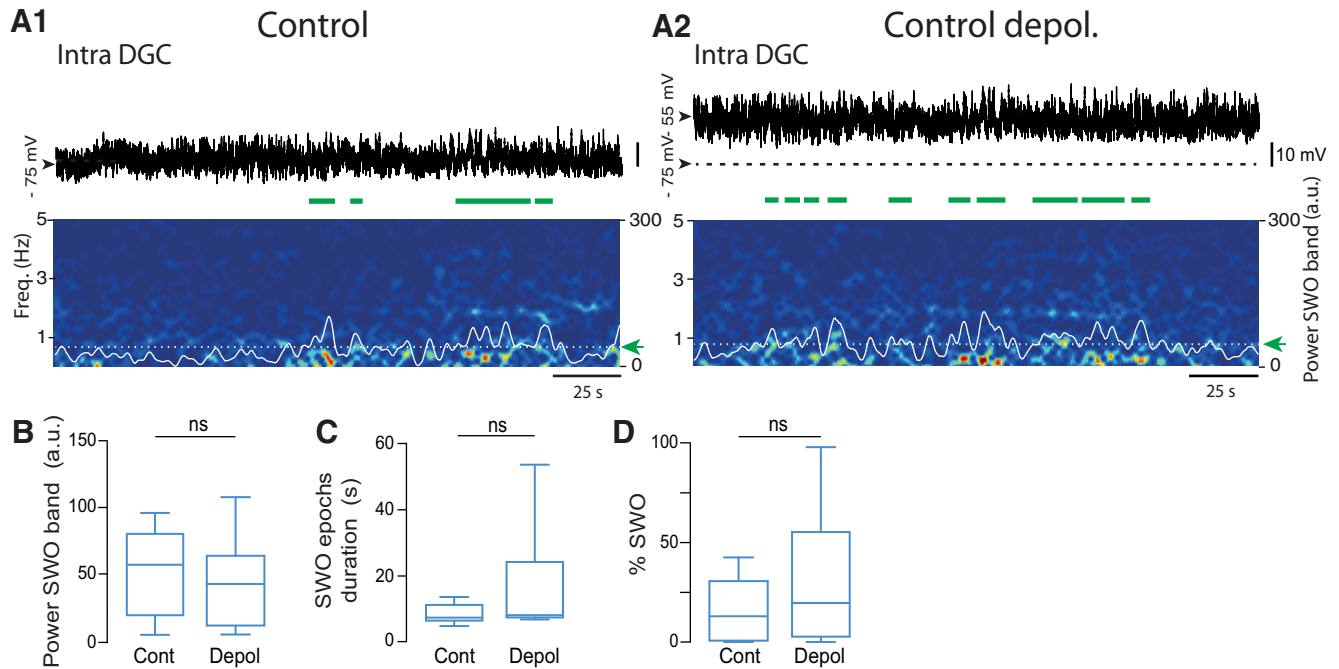
Figure 7. Lack of a significant increase in slow oscillations in the membrane potential of dentate granule cells by depolarization in control rats. **A1**, **A2**, Top, Membrane potential of a dentate granule cell from a control rat before (**A1**) and after (**A2**) artificial depolarization through direct current injection to ~-55 mV (spikes digitally removed). Scale bar in **A1** is the same as in **A2**. Bottom, Corresponding time–frequency power spectrograms (5 s sliding window, in 0.2 s steps). Superimposed white lines represent the time-varying power in the SWO band (0.1–2 Hz). Dashed white line (green arrow) indicates the SWO detection threshold used to detect SWO epochs highlighted by green horizontal bars below the traces. **B**, Box plots of the mean power in the SWO band over all recorded cells ($n = 8$) and recording times before (Cont) and after (Depol) depolarization. $p = 0.43$[jj]; Paired Student's t test. **C**, Box plots of the mean duration of single intracellular SWO epochs before (Cont) and after (Depol) depolarization. $p = 0.44$[kk]; $n = 6$; Wilcoxon signed rank test. **D**, Box plots of the percentage of intracellular SWO before (Cont) and after (Depol) depolarization. $p = 0.24$[ll]; $n = 8$; Paired Student's t test. ns, $p > 0.05$. For a description of box plots, see the legend of Figure 3.

could result from the spontaneous activation of intrinsically bursting neurons in layer V of cortex (Le Bon-Jego and Yuste, 2007; Lőrincz et al., 2015). Once an UP state is triggered, a barrage of synaptic excitatory and inhibitory inputs, occurring during the full duration of the UP state, contributes to its steady nature (Shu et al., 2003; Haider et al., 2006; Rudolph et al., 2007). This supposes a network with strong recurrent excitation (Sanchez-Vives and McCormick, 2000; Cossart et al., 2003) as well as feedback inhibition resulting from fast spiking basket cells activated during UP states (Shu et al., 2003; Fanselow and Connors, 2010; Massi et al., 2012; Tahvildari et al., 2012). The end of the UP state has been proposed to result from synaptic depression (Bazhenov et al., 2002; Holcman and Tsodyks, 2006), the buildup of activity-dependent potassium conductances (Sanchez-Vives and McCormick, 2000; Compte et al., 2003), and the activation of inhibitory interneurons (Shu et al., 2003) acting through GABA$_A$ (Lemieux et al., 2015) and/or GABA$_B$ (Parga and Abbott, 2007; Mann et al., 2009) receptors.

The lack of strong UP/DOWN state dynamics in control DGCs could result from the strong local inhibitory circuit of the dentate gyrus (Acsády et al., 1998; Nitz and Mc-Naughton, 2004; Ewell and Jones, 2010; Sambandan et al., 2010) together with strong dendritic filtering (Soltesz et al., 1995; Schmidt-Hieber et al., 2007; Krueppel et al.,

2011) that dampen the impact of excitatory inputs coming from layer II cells of the entorhinal cortex. In post-SE rats, however, the level of inhibition in DGCs is reduced during the latent period of TLE, notably at dendritic sites controlling inputs from the entorhinal cortex (Kobayashi and Buckmaster, 2003), presumably as a result of the early loss of several types of inhibitory interneurons in the dentate gyrus (Sloviter, 1987; Houser and Esclapez, 1996). In addition, excitatory inputs from layer II cells of the entorhinal cortex are increased 5 d post-SE as a result of decreased inhibition within the entorhinal cortex (Kobayashi et al., 2003). This imbalance in the excitatory/inhibitory drive could contribute to the strong UP/DOWN state V_m dynamics and firing observed in DGCs post-SE. Furthermore, at this early stage of epileptogenesis a switch of E(GABA) toward excitation has been reported (Pathak et al., 2007).

Alternatively, the absence of strong UP/DOWN state dynamics in control DGCs could result from the absence of a direct recurrent excitatory circuit in the dentate gyrus. Indeed, control DGCs only make indirect excitatory connections onto their peers through activation of mossy cells and need to fire at a sufficiently high rate to be able to discharge their targets (Henze et al., 2002). However, the axons of DGCs (the mossy fibers) sprout after status epilepticus to form a recurrent excitatory feedback circuit within the den-
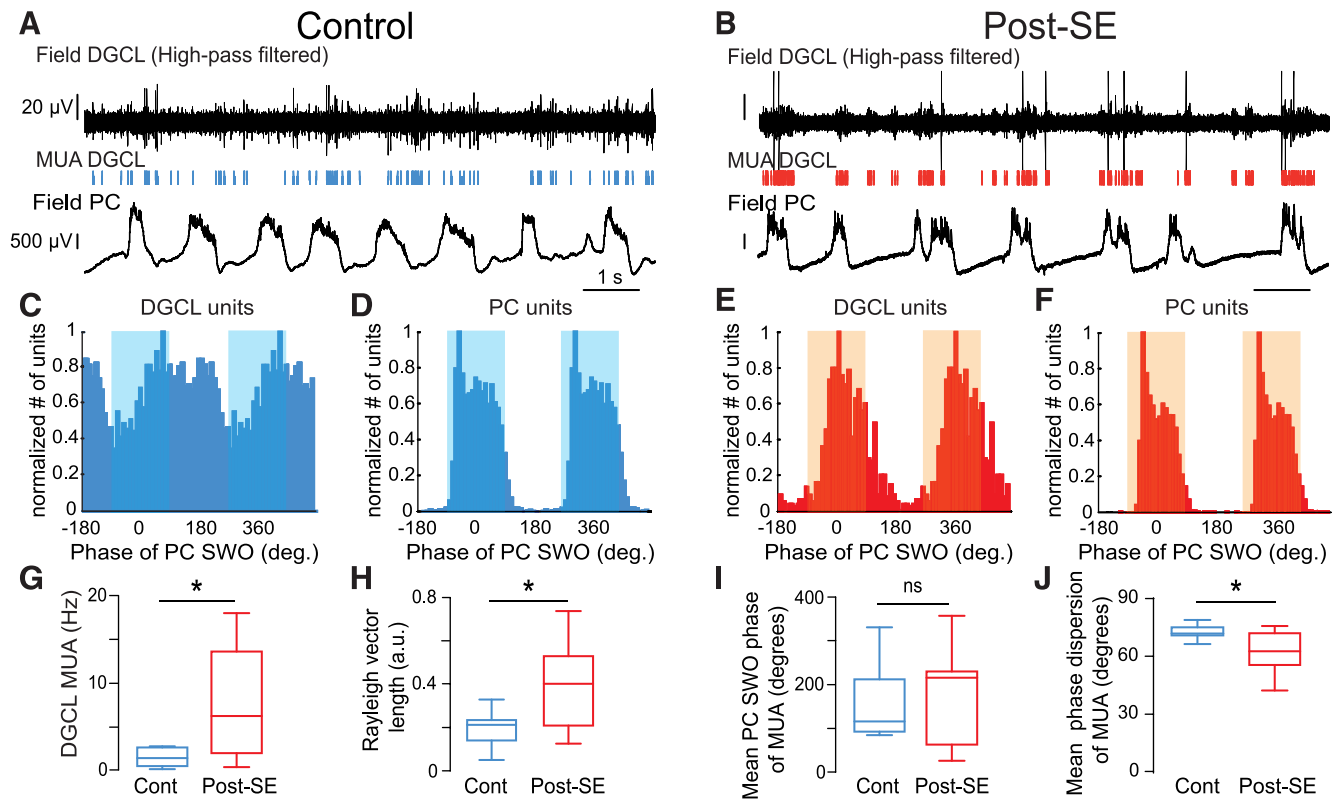
Figure 8. Increased rate and slow temporal modulation of multiunit activity in the dentate granule cell layer in post-SE vs control rats. *A*, *B*, High-pass-filtered (1000 Hz) local field potential recording in the dentate granule cell layer (DGCL; top) showing MUA (vertical bars) and simultaneously recorded local field potential in the parietal cortex (PC; bottom) in a control rat (*A*) and a post-SE rat (*B*). The scale bar values in *B* are the same as in *A*. *C*, *D*, Phase histogram of MUA from the recording shown in *A* (*C*) and simultaneously recorded in the parietal cortex (*D*). The blue-shaded area depicts the UP phase of SWO in the parietal cortex. *E*, *F*, Same layout as *C* and *D* for the recordings illustrated in *B*. The orange-shaded area depicts the UP phase of the SWO in the parietal cortex. *G*, Box plots of the frequency of MUA recorded in the DGCL. n = 7 control and n = 17 post-SE rats in this and all subsequent panels. *H*, Box plots of the length of Rayleigh vector of MUA recorded in the DGCL in control and post-SE rats. *I*, Box plots of the preferred phase of MUA recorded in the DGCL for all recordings in control and post-SE rats in reference to SWO recorded in the PC. *J*, Box plots of the dispersion of DGCL MUA around the mean phase of SWO recorded in the PC in control and post-SE rats. Ns, $p > 0.05$; ∗$p < 0.05$. For a description of box plots, see the legend of Figure 3.

tate gyrus not present in controls (Tauck and Nadler, 1985; Represa et al., 1987; Scharfman et al., 2003; Epsztein et al., 2005), which increases the excitability of DGCs (Artinian et al., 2011). These recurrent fibers result in part from the aberrant development of adult-born DGCs induced by the status epilepticus (Kron et al., 2010). This process is likely to be increased in our conditions because we use relatively young animals with a high level of adult neurogenesis and increased plasticity (Kuhn et al., 1996). Mossy fiber sprouting increases with time post-SE. It can already be observed during the latent period, but in a smaller proportion compared with the chronic stage (Wuarin and Dudek, 2001). Interestingly, computational work showed that even a low degree of mossy fiber sprouting can have a strong effect on network dynamics in a context of reduced inhibition (Santhakumar et al., 2005).

Sleep slow oscillation, UP/DOWN states, and epilepsy
Epileptic discharges in focal epilepsy are frequently observed during non-rapid eye movement sleep (Malow

et al., 1998). Most previous studies *in vivo* have focused on the impact of SWO on pathological activities, such as interictal epileptiform discharges or "UP spikes" (de Guzman et al., 2010; Bragin et al., 2012; Frauscher et al., 2015). No studies have analyzed the impact of the SWO itself on the V_m of principal cells in this pathological condition. Bragin et al. (2012) reported a decrease in the frequency of the field SWO recorded extracellularly in the dentate gyrus of chronically epileptic mice, due to an increased duration of both active and silent network phases. In our study, we tested the impact of the field neocortical SWO directly on the V_m of DGCs. We observed an increased duration and power of the V_m slow-oscillation of DGCs in post-SE versus control rats. Furthermore, the peak frequency of intracellular V_m slow oscillation was higher in the post-SE than the control condition (Fig. 2D). This frequency difference probably results from the fact that in controls, the V_m slow-oscillation of DGCs is poorly temporally coupled with the neocortical field activity (Fig. 5E). On the other hand, the V_m slow-oscillation of DGCs in post-SE rats is highly
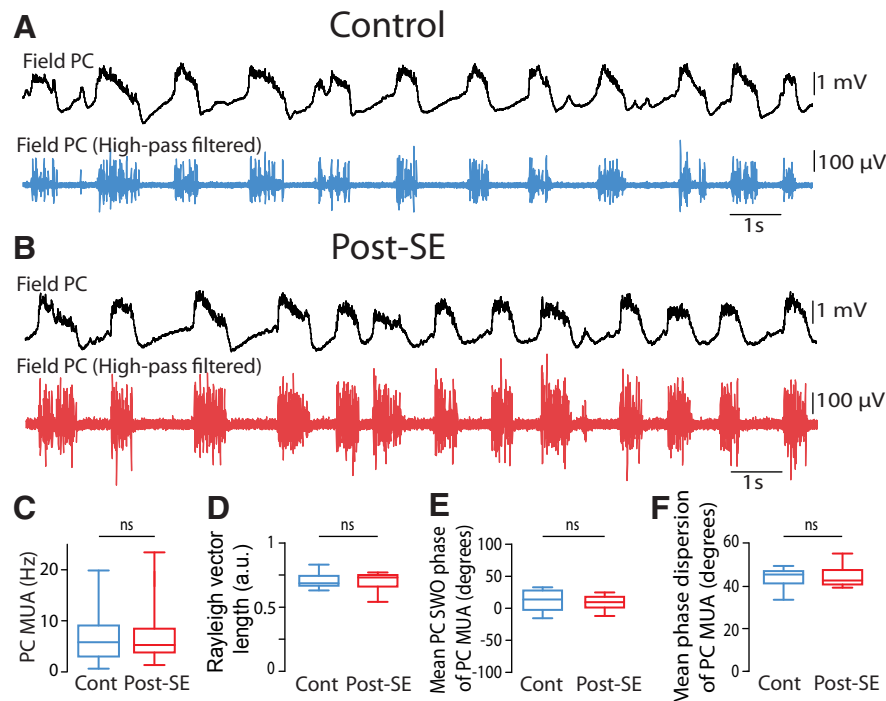
A   Control

Field PC

                                                    |1 mV

Field PC (High-pass filtered)

                                                    |100 µV

                                              |——| 1s

B   Post-SE

Field PC

                                                    |1 mV

Field PC (High-pass filtered)

                                                    |100 µV

                                              |——| 1s

Figure 9. Modulation of neocortical multiunit activity by the slow neocortical oscillation in control and post-SE rats. **A**, **B**, Raw (top, black) and high-pass filtered (1000 Hz, bottom) local field potential showing MUA recorded in the parietal cortex from a control rat (**A**) and a post-SE rat (**B**). **C**, Box plots of the frequency of MUA recorded in the parietal cortex. $n = 14$ control rats and $n = 17$ post-SE rats in this and all subsequent panels. **D**, Box plots of the length of the Rayleigh vector in control and post-SE conditions. **E**, Box plots of preferred SWO phase of PC MUA in control and post-SE conditions. **F**, Box plots of the dispersion of PC MUA around the mean SWO phase for control and post-SE conditions. ns, $p > 0.05$. For a description of box plots, see the legend of Figure 3.

temporally coupled to the neocortical field SWO (Fig. 5*E*) and oscillates at the same frequency (compare Figs. 2*D*, 4*D*, red traces). Thus, the difference we observed between the V_m slow-oscillation frequencies likely reflects an increased temporal coupling in the post-SE condition rather than an absolute change in the frequency of the neocortical field SWO, which is not different (Fig. 4*D*).

The only study on the consequences of a status epilepticus on intracellular UP/DOWN state V_m dynamics was performed *in vitro* using neocortical slices (Gerkin et al., 2010). In that work, the frequency of UP states recorded in layer 2/3 neocortical pyramidal neurons was increased 24 h after a picrotoxin-induced seizure. This resulted from shorter DOWN states, associated with increased single-cell intrinsic excitability. Indeed, a higher number of action potentials was generated per UP state following seizure induction. However, in our study, the frequency of the SWO was not modified in the parietal cortex, and neocortical MUA activity was not increased, suggesting no change of neocortical excitability during the latent period in our model of TLE. In contrast to neocortical neurons in controls, which display strong UP/DOWN state dynamics, the Vm of control DGCs was only weakly modulated by the neocortical SWO and clear UP/DOWN dynamics were rarely observed. However, several days after the induction of the status epilepticus, clear UP/DOWN V_m dynamics could be seen. The scarcity of UP/DOWN V_m dynamics in controls and the abundance fol-

lowing the SE points to a morphofunctional change in the network, rather than a change in the intrinsic excitability of DGCs, as a possible explanation. In line with this hypothesis, increasing single-cell excitability through direct current injection via the recording pipette was not enough to induce SWO in the V_m of control DGCs. Furthermore, the number of spikes per neocortical UP phase was not modified in DGCs from post-SE rats, arguing against an increased intrinsic excitability.

Functional consequences of higher UP/DOWN state V_m dynamics in DGCs from post-SE rats

At the entrance of the hippocampus, the dentate gyrus has been proposed to transform dense neocortical inputs into sparse and specific neuronal representations (Chawla et al., 2005; Acsády and Kali, 2007; Leutgeb et al., 2007), which can then be imposed onto their downstream CA3 pyramidal cells target for subsequent storage (McNaughton and Morris, 1987; Treves and Rolls, 1992). In accordance with this function, DGCs are particularly reluctant to fire action potentials both *in vitro* (Scharfman, 1991; Ewell and Jones, 2010) and *in vivo* (Jung and McNaughton, 1993; Penttonen et al., 1997; Leutgeb et al., 2007; Neunuebel and Knierim, 2012; Pernía-Andrade and Jonas, 2014; Diamantaki et al., 2016; Kowalski et al., 2016). By bringing DGCs closer to firing threshold, UP states likely facilitated the generation of action potentials. Indeed, 75% of DGCs were spontaneously firing in

post-SE rats against 20% in controls, and the firing rate of individual cells was strongly increased. This increase likely results from the increased number of UP states rather than increased intrinsic excitability of DGCs, because the number of spikes generated by individual UP states was not different between control and post-SE rats. The MUA recorded in the dentate granule cell layer was not only increased, but also was more strongly and precisely paced by the neocortical SWO in post-SE versus control rats. Previous studies (Mori et al., 2004) have shown that DGCs can have either an inhibitory (at low firing rate) or an excitatory (at high firing rate) impact on downstream targets. In our recordings, the increase in the firing rate of individual cells, although substantial, was still too low to allow faithful excitation of CA3 pyramidal cells during the UP state by individual DGCs (Henze et al., 2002). The increased frequency could instead enhance their inhibitory impact on CA3 activity during the neocortical UP state already observed in controls (Isomura et al., 2006). On the other hand, because more DGCs are firing spontaneously and because their firing is more strongly synchronized by the SWO, the likelihood of having an ensemble of DGCs coactive will be increased. Altogether, these cells could have a significant impact on single-CA3 pyramidal cell firing behavior. The net impact of these changes on downstream targets remains to be investigated but is difficult to anticipate because CA3 and CA1 networks are themselves profoundly modified in TLE.

The slow cortical oscillation is able to bias the occurrence of hippocampal sharp-wave/ripple events (Sirota et al., 2003; Battaglia et al., 2004; Mölle et al., 2006; Logothetis et al., 2012) and is important for hippocampus-dependent declarative memory consolidation in humans (Marshall et al., 2006). Future studies will tell whether the increased modulation of the activity of DGCs by the slow cortical oscillation that we report has an incidence on the replay and consolidation of information during sleep in patients with TLE.

References

Acsády L, Kali S (2007) Models, structure, function: the transformation of cortical signals in the dentate gyrus. Prog Brain Res 163: 577-599. CrossRef Medline

Acsády L, Kamondi A, Sík A, Freund T, Buzsáki G (1998) GABAergic cells are the major postsynaptic targets of mossy fibers in the rat hippocampus. J Neurosci 18:3386-3403. Medline

Artinian J, Peret A, Marti G, Epsztein J, Crépel V (2011) Synaptic kainate receptors in interplay with INaP shift the sparse firing of dentate granule cells to a sustained rhythmic mode in temporal lobe epilepsy. J Neurosci 31:10811-10818. CrossRef Medline

Battaglia FP, Sutherland GR, McNaughton BL (2004) Hippocampal sharp wave bursts coincide with neocortical "up-state" transitions. Learn Mem 11:697-704. CrossRef Medline

Bazhenov M, Timofeev I, Steriade M, Sejnowski TJ (2002) Model of thalamocortical slow-wave sleep oscillations and transitions to activated states. J Neurosci 22:8691-8704. Medline

Behr J, Lyson KJ, Mody I (1998) Enhanced propagation of epileptiform activity through the kindled dentate gyrus. J Neurophysiol 79:1726-1732. Medline

Bragin A, Benassi SK, Engel J Jr (2012) Patterns of the UP-Down state in normal and epileptic mice. Neuroscience 225:76-87. CrossRef Medline

Burwell RD, Amaral DG (1998) Cortical afferents of the perirhinal, postrhinal, and entorhinal cortices of the rat. J Comp Neurol 398:179-205. Medline

Chauvel S, Volgushev M, Timofeev I (2010) Origin of active states in local neocortical networks during slow sleep oscillation. Cereb Cortex 20:2660-2674. CrossRef Medline

Chauvette S, Crochet S, Volgushev M, Timofeev I (2011) Properties of slow oscillation during slow-wave sleep and anesthesia in cats. J Neurosci 31:14998-15008. CrossRef Medline

Chauvière L, Rafrafi N, Thinus-Blanc C, Bartolomei F, Esclapez M, Bernard C (2009) Early deficits in spatial memory and theta rhythm in experimental temporal lobe epilepsy. J Neurosci 29:5402-5410. CrossRef Medline

Chawla MK, Guzowski JF, Ramirez-Amaya V, Lipa P, Hoffman KL, Marriott LK, Worley PF, McNaughton BL, Barnes CA (2005) Sparse, environmentally selective expression of Arc RNA in the upper blade of the rodent fascia dentata by brief spatial experience. Hippocampus 15:579-586. CrossRef Medline

Collins DR, Pelletier JG, Paré D (2001) Slow and fast (gamma) neuronal oscillations in the perirhinal cortex and lateral amygdala. J Neurophysiol 85:1661-1672. Medline

Compte A, Sanchez-Vives MV, McCormick DA, Wang XJ (2003) Cellular and network mechanisms of slow oscillatory activity (<1 Hz) and wave propagations in a cortical network model. J Neurophysiol 89:2707-2725. CrossRef Medline

Cossart R, Aronov D, Yuste R (2003) Attractor dynamics of network UP states in the neocortex. Nature 423:283-288. CrossRef Medline

Cowan RL, Wilson CJ (1994) Spontaneous firing patterns and axonal projections of single corticostriatal neurons in the rat medial agranular cortex. J Neurophysiol 71:17-32. Medline

Crochet S, Petersen CC (2006) Correlating whisker behavior with membrane potential in barrel cortex of awake mice. Nat Neurosci 9:608-610. CrossRef Medline

de Guzman PH, Nazer F, Dickson CT (2010) Short-duration epileptic discharges show a distinct phase preference during ongoing hippocampal slow oscillations. J Neurophysiol 104:2194-2202. CrossRef Medline

Diamantaki M, Frey M, Preston-Ferrer P, Burgalossi A (2016) Priming spatial activity by single-cell stimulation in the dentate gyrus of freely moving rats. Curr Biol 26:536-541. CrossRef Medline

Dudek FE, Sutula TP (2007) Epileptogenesis in the dentate gyrus: a critical perspective. Prog Brain Res 163:755-773. CrossRef Medline

Epsztein J, Represa A, Jorquera I, Ben-Ari Y, Crépel V (2005) Recurrent mossy fibers establish aberrant kainate receptor-operated synapses on granule cells from epileptic rats. J Neurosci 25:8229-8239. CrossRef Medline

Ewell LA, Jones MV (2010) Frequency-tuned distribution of inhibition in the dentate gyrus. J Neurosci 30:12597-12607. CrossRef Medline

Fanselow EE, Connors BW (2010) The roles of somatostatin-expressing (GIN) and fast-spiking inhibitory interneurons in UP-DOWN states of mouse neocortex. J Neurophysiol 104:596-606. CrossRef Medline

Fisher NI (1993) Statistical analysis of circular data. Cambridge, U.K.: Cambridge UP.

Frauscher B, von EN, Ferrari-Marinho T, Avoli M, Dubeau F, Gotman J (2015) Facilitation of epileptic activity during sleep is mediated by high amplitude slow waves. Brain 138:1629-1641. CrossRef Medline

Gerkin RC, Clem RL, Shruti S, Kass RE, Barth AL (2010) Cortical up state activity is enhanced after seizures: a quantitative analysis. J Clin Neurophysiol 27:425-432. CrossRef Medline

Hahn TT, Sakmann B, Mehta MR (2006) Phase-locking of hippocampal interneurons' membrane potential to neocortical up-down states. Nat Neurosci 9:1359-1361. CrossRef Medline

Hahn TT, Sakmann B, Mehta MR (2007) Differential responses of hippocampal subfields to cortical up-down states. Proc Natl Acad Sci U S A 104:5169-5174. CrossRef Medline

Hahn TT, McFarland JM, Berberich S, Sakmann B, Mehta MR (2012) Spontaneous persistent activity in entorhinal cortex modulates cortico-hippocampal interaction *in vivo*. Nat Neurosci 15:1531-1538. CrossRef Medline

Haider B, Duque A, Hasenstaub AR, McCormick DA (2006) Neocortical network activity *in vivo* is generated through a dynamic balance of excitation and inhibition. J Neurosci 26:4535-4545. CrossRef Medline

Hartigan JA, Hartigan PM (1985) The dip test of unimodality. Ann Stat 13:70-84. CrossRef

Henze DA, Wittner L, Buzsáki G (2002) Single granule cells reliably discharge targets in the hippocampal CA3 network *in vivo*. Nat Neurosci 5:790-795. CrossRef Medline

Holcman D, Tsodyks M (2006) The emergence of Up and Down states in cortical networks. PLoS Comput Biol 2:e23. CrossRef Medline

Houser CR, Esclapez M (1996) Vulnerability and plasticity of the GABA system in the pilocarpine model of spontaneous recurrent seizures. Epilepsy Res 26:207-218. Medline

Isomura Y, Sirota A, Ozen S, Montgomery S, Mizuseki K, Henze DA, Buzsáki G (2006) Integration and segregation of activity in entorhinal-hippocampal subregions by neocortical slow oscillations. Neuron 52:871-882. CrossRef Medline

Jung MW, McNaughton BL (1993) Spatial selectivity of unit activity in the hippocampal granular layer. Hippocampus 3:165-182. CrossRef Medline

Kobayashi M, Buckmaster PS (2003) Reduced inhibition of dentate granule cells in a model of temporal lobe epilepsy. J Neurosci 23:2440-2452.

Kobayashi M, Wen X, Buckmaster PS (2003) Reduced inhibition and increased output of layer II neurons in the medial entorhinal cortex in a model of temporal lobe epilepsy. J Neurosci 23:8471-8479. Medline

Kowalski J, Gan J, Jonas P, Pernía-Andrade AJ (2016) Intrinsic membrane properties determine hippocampal differential firing pattern in vivo in anesthetized rats. Hippocampus 26:668-682. CrossRef Medline

Kron MM, Zhang H, Parent JM (2010) The developmental stage of dentate granule cells dictates their contribution to seizure-induced plasticity. J Neurosci 30:2051-2059. CrossRef Medline

Krook-Magnuson E, Armstrong C, Bui A, Lew S, Oijala M, Soltesz I (2015) In vivo evaluation of the dentate gate theory in epilepsy. J Physiol 593:2379-2388. CrossRef Medline

Krueppel R, Remy S, Beck H (2011) Dendritic integration in hippocampal dentate granule cells. Neuron 71:512-528. CrossRef Medline

Kuhn HG, Dickinson-Anson H, Gage FH (1996) Neurogenesis in the dentate gyrus of the adult rat: age-related decrease of neuronal progenitor proliferation. J Neurosci 16:2027-2033. Medline

Le Bon-Jego M, Yuste R (2007) Persistently active, pacemaker-like neurons in neocortex. Front Neurosci 1:123-129. CrossRef Medline

Lemieux M, Chauvette S, Timofeev I (2015) Neocortical inhibitory activities and long-range afferents contribute to the synchronous onset of silent states of the neocortical slow oscillation. J Neurophysiol 113:768-779. CrossRef Medline

Leutgeb JK, Leutgeb S, Moser MB, Moser EI (2007) Pattern separation in the dentate gyrus and CA3 of the hippocampus. Science 315:961-966. CrossRef Medline

Loewenstein Y, Mahon S, Chadderton P, Kitamura K, Sompolinsky H, Yarom Y, Häusser M (2005) Bistability of cerebellar Purkinje cells modulated by sensory stimulation. Nat Neurosci 8:202-211. CrossRef Medline

Logothetis NK, Eschenko O, Murayama Y, Augath M, Steudel T, Evrard HC, Besserve M, Oeltermann A (2012) Hippocampal-cortical interaction during periods of subcortical silence. Nature 491:547-553. CrossRef Medline

Lőrincz ML, Gunner D, Bao Y, Connelly WM, Isaac JT, Hughes SW, Crunelli V (2015) A distinct class of slow (~0.2-2 Hz) intrinsically bursting layer 5 pyramidal neurons determines UP/DOWN state

dynamics in the neocortex. J Neurosci 35:5442-5458. CrossRef Medline

Mahon S, Vautrelle N, Pezard L, Slaght SJ, Deniau JM, Chouvet G, Charpier S (2006) Distinct patterns of striatal medium spiny neuron activity during the natural sleep-wake cycle. J Neurosci 26:12587-12595. CrossRef Medline

Malow BA, Lin X, Kushwaha R, Aldrich MS (1998) Interictal spiking increases with sleep depth in temporal lobe epilepsy. Epilepsia 39:1309-1316. Medline

Mann EO, Kohl MM, Paulsen O (2009) Distinct roles of GABA$_A$ and GABA$_B$ receptors in balancing and terminating persistent cortical activity. J Neurosci 29:7513-7518. CrossRef Medline

Margrie TW, Brecht M, Sakmann B (2002) In vivo, low-resistance, whole-cell recordings from neurons in the anaesthetized and awake mammalian brain. Pflugers Arch 444:491-498. CrossRef Medline

Marshall L, Helgadóttir H, Mölle M, Born J (2006) Boosting slow oscillations during sleep potentiates memory. Nature 444:610-613. CrossRef Medline

Massi L, Lagler M, Hartwich K, Borhegyi Z, Somogyi P, Klausberger T (2012) Temporal dynamics of parvalbumin-expressing axo-axonic and basket cells in the rat medial prefrontal cortex in vivo. J Neurosci 32:16496-16502. CrossRef Medline

McNaughton BL, Morris RGM (1987) Hippocampal synaptic enhancement and information storage within a distributed memory system. Trends Neurosci 10:408-415. CrossRef

Mölle M, Yeshenko O, Marshall L, Sara SJ, Born J (2006) Hippocampal sharp wave-ripples linked to slow oscillations in rat slow-wave sleep. J Neurophysiol 96:62-70. CrossRef Medline

Mori M, Abegg MH, Gähwiler BH, Gerber U (2004) A frequency-dependent switch from inhibition to excitation in a hippocampal unitary circuit. Nature 431:453-456. CrossRef Medline

Nagao T, Alonso A, Avoli M (1996) Epileptiform activity induced by pilocarpine in the rat hippocampal-entorhinal slice preparation. Neuroscience 72:399-408. Medline

Neunuebel JP, Knierim JJ (2012) Spatial firing correlates of physiologically distinct cell types of the rat dentate gyrus. J Neurosci 32:3848-3858. CrossRef Medline

Nitz D, McNaughton B (2004) Differential modulation of CA1 and dentate gyrus interneurons during exploration of novel environments. J Neurophysiol 91:863-872. CrossRef Medline

Parga N, Abbott LF (2007) Network model of spontaneous activity exhibiting synchronous transitions between up and down States. Front Neurosci 1:57-66. CrossRef Medline

Pathak HR, Weissinger F, Terunuma M, Carlson GC, Hsu FC, Moss SJ, Coulter DA (2007) Disrupted dentate granule cell chloride regulation enhances synaptic excitability during development of temporal lobe epilepsy. J Neurosci 27:14012-14022. CrossRef Medline

Penttonen M, Kamondi A, Sik A, Acsády L, Buzsáki G (1997) Feed-forward and feed-back activation of the dentate gyrus in vivo during dentate spikes and sharp wave bursts. Hippocampus 7:437-450. CrossRef Medline

Pernía-Andrade AJ, Jonas P (2014) Theta-gamma-modulated synaptic currents in hippocampal granule cells in vivo define a mechanism for network oscillations. Neuron 81:140-152. CrossRef Medline

Represa A, Tremblay E, Ben-Ari Y (1987) Kainate binding sites in the hippocampal mossy fibers: localization and plasticity. Neuroscience 20:739-748. Medline

Ros H, Sachdev RN, Yu Y, Sestan N, McCormick DA (2009) Neocortical networks entrain neuronal circuits in cerebellar cortex. J Neurosci 29:10309-10320. CrossRef Medline

Rudolph M, Pospischil M, Timofeev I, Destexhe A (2007) Inhibition determines membrane potential dynamics and controls action potential generation in awake and sleeping cat cortex. J Neurosci 27:5280-5290. CrossRef Medline

Sales-Carbonell C, Rueda-Orozco PE, Soria-Gómez E, Buzsáki G, Marsicano G, Robbe D (2013) Striatal GABAergic and cortical glutamatergic neurons mediate contrasting effects of cannabi-

noids on cortical network synchrony. Proc Natl Acad Sci U S A 110:719-724. CrossRef Medline

Sambandan S, Sauer JF, Vida I, Bartos M (2010) Associative plasticity at excitatory synapses facilitates recruitment of fast-spiking interneurons in the dentate gyrus. J Neurosci 30:11826-11837. CrossRef Medline

Sanchez-Vives MV, McCormick DA (2000) Cellular and network mechanisms of rhythmic recurrent activity in neocortex. Nat Neurosci 3:1027-1034. CrossRef Medline

Santhakumar V, Aradi I, Soltesz I (2005) Role of mossy fiber sprouting and mossy cell loss in hyperexcitability: a network model of the dentate gyrus incorporating cell types and axonal topography. J Neurophysiol 93:437-453. CrossRef Medline

Scharfman HE (1991) Dentate hilar cells with dendrites in the molecular layer have lower thresholds for synaptic activation by perforant path than granule cells. J Neurosci 11:1660-1673.

Scharfman HE, Sollas AL, Berger RE, Goodman JH (2003) Electrophysiological evidence of monosynaptic excitatory transmission between granule cells after seizure-induced mossy fiber sprouting. J Neurophysiol 90:2536-2547. CrossRef Medline

Schmidt-Hieber C, Jonas P, Bischofberger J (2007) Subthreshold dendritic signal processing and coincidence detection in dentate gyrus granule cells. J Neurosci 27:8430-8441. CrossRef Medline

Shu Y, Hasenstaub A, McCormick DA (2003) Turning on and off recurrent balanced cortical activity. Nature 423:288-293. CrossRef Medline

Sirota A, Csicsvari J, Buhl D, Buzsáki G (2003) Communication between neocortex and hippocampus during sleep in rodents. Proc Natl Acad Sci U S A 100:2065-2069. CrossRef Medline

Sloviter RS (1987) Decreased hippocampal inhibition and a selective loss of interneurons in experimental epilepsy. Science 235:73-76. Medline

Soltesz I, Smetters DK, Mody I (1995) Tonic inhibition originates from synapses close to the soma. Neuron 14:1273-1283. Medline

Steriade M, Nuñez A, Amzica F (1993) A novel slow (< 1 Hz) oscillation of neocortical neurons *in vivo*: depolarizing and hyperpolarizing components. J Neurosci 13:3252-3265. Medline

Steriade M, Timofeev I, Grenier F (2001) Natural waking and sleep states: a view from inside neocortical neurons. J Neurophysiol 85:1969-1985. Medline

Tahvildari B, Wölfel M, Duque A, McCormick DA (2012) Selective functional interactions between excitatory and inhibitory cortical neurons and differential contribution to persistent activity of the slow oscillation. J Neurosci 32:12165-12179. CrossRef Medline

Tauck DL, Nadler JV (1985) Evidence of functional mossy fiber sprouting in hippocampal-formation of kainic acid-treated rats. J Neurosci 5:1016-1022. Medline

Timofeev I, Grenier F, Bazhenov M, Sejnowski TJ, Steriade M (2000) Origin of slow cortical oscillations in deafferented cortical slabs. Cereb Cortex 10:1185-1199. Medline

Timofeev I, Grenier F, Steriade M (2001) Disfacilitation and active inhibition in the neocortex during the natural sleep-wake cycle: an intracellular study. Proc Natl Acad Sci U S A 98:1924-1929. CrossRef Medline

Treves A, Rolls ET (1992) Computational constraints suggest the need for two distinct input systems to the hippocampal CA3 network. Hippocampus 2:189-199. CrossRef Medline

Volgushev M, Chauvette S, Mukovski M, Timofeev I (2006) Precise long-range synchronization of activity and silence in neocortical neurons during slow-wave sleep. J Neurosci 26:5665-5672.

Wilson CJ, Kawaguchi Y (1996) The origins of two-state spontaneous membrane potential fluctuations of neostriatal spiny neurons. J Neurosci 16:2397-2410. Medline

Wolansky T, Clement EA, Peters SR, Palczak MA, Dickson CT (2006) Hippocampal slow oscillation: a novel EEG state and its coordination with ongoing neocortical activity. J Neurosci 26:6213-6229. CrossRef Medline

Wuarin JP, Dudek FE (2001) Excitatory synaptic input to granule cells increases with time after kainate treatment. J Neurophysiol 85: 1067-1077. Medline